MORPHOLOGICAL EVALUATION OF 1-SITE POLYCRYSTALLINE MODELS

by

Mustafa Şengör

B.S., Mechanical Engineering, Boğaziçi University, 2010

Submitted to the Institute for Graduate Studies in
Science and Engineering in partial fulfillment of
the requirements for the degree of
Master of Science

Graduate Program in Mechanical Engineering

Boğaziçi University

2013

This study is dedicated to my beloved mother and father .

ACKNOWLEDGEMENTS

It is impossible for me to thank my parents Melihat and Nurettin Şengör enough for supporting me during my life. I also would like to thank especially to my dear brothers Arif, Sinan, Ömer and little sister Gülseda, because sometimes human beings require empathy more than a physical or mental support.

I would like to express that I feel honored to be a student of Assist. Prof. C.Can Aydıner. He contributed to my scientific development considerably and I obtained unforgettable life lessons during this time.

I would like to thank the members of the committee, Prof. Günay Anlaş and Assist. Prof. Çağrı Diner, for their comments and suggestions in the development of this thesis.

It is impossible to state my friends one by one. But precious friends of “Last 8-horses” and invaluable “İLKAD” members are holding an important place in my life. And I also cannot forget the assistance and collaboration of dear “Hüdai” members.

I would like to express my sincere appreciations to Gökalp Erbeyoğlu, whenever I went all to pot, he is always ready for to help. Lastly, I have to thank to M. Ayça Telemez for showing me the other side of the road.

ABSTRACT

MORPHOLOGICAL EVALUATION OF 1-SITE POLYCRYSTALLINE MODELS

Mesoscale models consider grain level interactions. Unlike continuum models, they account for the discontinuities stemming from the elastic anisotropy of the crystallites in addition to the directional nature of the dislocation slip. Load fractions on individual grains are decided by considering the individual neighborhood of grains (n-site models), or by making unifying assumptions ignoring the specific neighborhood (1-site models). 1-site models are typically incapable of incorporating the morphology of the grain neighborhood except for the self-consistent models (SCM). This thesis investigates the tools and model adaptations to make self-consistent models capable of modeling single-phase and multi-phase polycrystals with pronounced morphological features. Modeling the effects of these features with 1-site models allow avoiding the more expensive and complicated finite element analyses. To this end, a flexible, object-oriented, Python® based software framework is engendered, called APMF (Adaptable Point Model Framework). APMF can (i) accommodate conventional single-phase applications, (ii) extended with multi-phase materials and (iii) allows extension to any desired constitutive rule or polycrystalline interaction. Models created with APMF are verified with several test cases of single-phase and multi-phase structures. Among 1-site models, SCM implements morphology by adjusting the radii and orientations of the Eshelby ellipsoid (inclusion). The current APMF implementation adds the capacity to assign these parameters independently for each grain. By using limiting shapes of Eshelby ellipsoid (namely, sphere, needle, and disc) and comparing with the simplistic isostrain/isostress rules, the effect of the structured (non-random) morphologies on the behavior of the polycrystals are simulated. As a multi-phase application, residual strains inside a two-phase Cu/Nb bilayer is studied by applying thermally induced eigenstrain on the Nb aggregate. In single-phase polycrystals, to model the interaction correctly, a one-to-one relation between the grain shape and the inclusion shape is observed. On the other hand, to capture the interaction correctly in two-phase materials having different grain shapes, APMF should be extended with hierarchic models.

ÖZET

1-KOMŞULU POLİ-KRİSTAL MODELLERİNİN MORFOLOJİK DEĞERLENDİRİLMESİ

Mezo-skaladaki modeller tanecik seviyesindeki etkileşimi göz önünde bulundururlar. Sürekli ortam modellerinden farklı olarak, kristaldeki elastik anizotropi ile plastik aktivitelerden kaynaklı süreksizlikleri hesaba katarlar. Tekil tanecikler üzerindeki yük fraksiyonlarına, taneciklerin mahalilndeki diğer taneciklerin hesaba katıldığı (n-komşulu) modeller ile ya da birleştirici varsayım yapıp tekil komuşu etkilerini görmezden gelen (1-komşulu) modeller ile karar verilir. Kendi içinde tutarlı modeller (SCM) haricinde 1-komşulu modeller morfolojik etkilerin değerlendirilmesinde limitlidir. Bu tez SCM'lerin tek fazlı ve çok fazlı polikristal deformasyonunu modelleyebilecek yeteneğe getirmek için gerekli olan araçları ve model adaptasyonlarını incelemektedir. Bariz morfolojilerin başarılı mezo-skala modellemeleri daha komplike ve masraflı olan sonlu eleman modellerinden kaçınmaya izin verir. Bu bağlamda, ayarlanabilir nokta model çerçevesi (APMF) isminde Python® da yazılmış, nesne-bazlı, esnek bir yazılım çerçevesi oluşturuldu. Bu yapı (i) hazırdaki uygulamalarla bağdaştırılabilir, (ii) çok-fazlı malzemeler ile genişletilmiş, ve (iii) istenilen polikristal model eklentisi yapmaya izin verir. APMF ile üretilmiş modeller tek ve çok fazlı birçok sayısal deney ile doğrulanmıştır. 1-komşulu modeller arasında SCM , Eshelby elipsoidinin (inklüzyon) yarı çapı ve oryantasyonunun ayarlaması ile morfolojiyi uygular. Şu anki APMF bu parametrelerin tek tek bütün tanecikler için bağımsız olarak uygulayabilir. Eshelby elipsoidinin limit şekilleri kullanılarak, (küre, iğne, ve disk şeklindeki) ve bunların yalın, eşit-gerilim/gerinim kuralları ile kıyaslayarak, rastgele olmayan morfolojilerin polikristal üzerindeki etkisi simule edildi. İki fazlı, iki katmanlı Cu/Nb'un içerisindeki kalıntı gerinimler, Nb kümesinin üzerinde termal olarak oluşturulmuş özgerinim çalışıldı. Tek fazlı polikristalde, doğru modelleme için, tanecik ile inklüzyon şekli arasında birebir ilişki olduğu gözlemlendi. Diğer yandan, APMF'nin herbir fazın farklı şekle sahip olduğu iki fazlı malzemelerin doğru modellenmesi için hiyerarşik modelleme ile geliştirilmesi gerektiği görüldü.

TABLE OF CONTENTS

LIST OF FIGURES

LIST OF TABLES

LIST OF SYMBOLS

A_c	4th order localization matrix of a crystal
b	X-ray beam
C	crystal coordinate system
C_c	Elastic stiffness of the single crystal
C_I	stiffness of the actual inhomogeneity
d	Grain size
d_{hkl}	Lattice distance among hkl family planes
E_{hkl}	Elastic modulus along <hkl> in a single crystal
f	Body force
f^s	Projector tensor which projects the strain rate tensors of the crystal to a shear strain rate for each active slip system
g	Orientation distribution function
$G_{ij}(\boldsymbol{r})$	Green function for a unit load where i is the ith component of the displacement and the j is the jth component of the applied unit force
$h^{ss'}$	Latent hardening where s≠s’
hkl	Miller indices of the crystallographic plane

k	Hall-Petch Slope
$\mathbf{k}$	Scattering vector
$\mathbf{k}_i$	Vector of the incident beam
$\mathbf{k}_o$	Vector of reflected beam
L	Macroscopic tangent stiffness
L^*	Effective modulus
L_c	Tangent stiffness of the single crystal
S	Eshelby tensor
S	sample coordinate system
$\boldsymbol{u}$	Displacement vector
α	Macroscopic thermal coefficient tensor
α_c	Crystal thermal coefficient tensor
$\dot{\gamma}^{\alpha}$	Shear strain rate of the α^{th} actual slip system
$\dot{\gamma}_*^{\alpha}$	Shear strain rate of the α^{th} geometrically possible slip system
ε_{ij}^{e}	Elastic strain

ε_{ij}^{*}	Transformation strain of the inclusion
$\dot{\varepsilon}$	Macroscopic strain rate
$\dot{\varepsilon}^{c}$	Strain rate of the inclusion
ε_{hkl}	Strain along hkl plane normal
σ_{ij}	Cauchy's stress tensor
σ_{y}	Yield stress
σ_{0}	Frictional stress required to move the dislocations´
σ_c	Crystal Stress
σ	Macroscopic Stress
σ_{hkl}	Stress along hkl plane normal
λ	X-ray wavelength
θ	X-ray incident angle
μ^{s}	Schmidt tensor
τ_{c}^{α}	Current shear strength of the α^{th} physically-activated slip system
τ_{c*}^{α}	Current shear strength of the α^{th} geometrically possible slip system
τ_{0}^{s}	Critical resolved shear stress of the s^{th} slip system

$\tau_1^s, \theta_0^s, \theta_1^s$	Voce Hardenıng parameters
Γ	Accumulated shear strain inside each grain
λ ,μ	Lame constants for isotropic elastic medium

LIST OF ACRONYMS/ABBREVIATIONS

2D	Two dimensional
APMF	Adaptable Point Model Framework
AR	Anisotropy ratio
BC	Boundary condition
BCC	Body-centered-cubic
CRSS	Critical resolved shear stress
CS	Coordinate system
EEI	Eshelby ellipsoidal inclusion
EPSC	Elasto-plastic self-consistent
FCC	Face-centered-cubic
HCP	Hexagonal-close-packed
HEM	Homogeneous equivalent medium
NA	Not Applicable
ND	Normal direction
ODF	Orientation distribution function
RD	Rolling direction
SCM	Self-Consistent Method
SEM	Scanning electron microscopy
VPSC	Visco-plastic self-consistent
XRD	X-ray diffraction

1. INTRODUCTION

1.1. Motivation

A polycrystalline aggregate is a material that is composed of many crystallites. Most of the bulk materials in engineering use are polycrystalline. Interactions in between the crystallites (grains) and constitutive behavior of individual crystallites govern the physical response of the aggregates. To capture the meso-micro scale stress-strain response of the aggregates, interaction and constitutive models are developed. With the resulting predictive capability, the redundancy in trial-and-error based experimental design is minimized. Continuum models explain variations inside the materials through continuous fields with no allowances for abrupt changes or discontinuities [1]. Hence, they neglect the discontinuities stemming from the anisotropy inside the polycrystals [2].

On the other hand meso-scale models, considers the slip plasticity or twinning mechanisms for individual grains that allow them to capture fundamental mechanisms of deformation directly. Meso-scale models can account for the individual neighborhood of grains (n-site) models, or make unifying assumptions ignoring the specific neighborhood (1-site models) by using [3-7]. An example for the n-site models is Finite Element Method (FEM) that directly models the geometry of all grains [8]. FEM is a powerful tool in considering the deformation stages of an aggregate. It considers a grain inside the aggregate whose behavior will depend on the different orientations of its specific neighbors. Given the elastic-plastic anisotropy of a typical crystallite, the grain and all its neighbors possess different elastic-plastic stiffnesses. Although FEM gives realistic results, it is (i) computationally very expensive and (ii) there is rarely sufficient experimental data on the combined morphology/orientation of the studied polycrystal to warrant FEM.

For obtaining orientation-specific representative results, 1-site models are good alternatives. Further, the analyses are much cheaper in terms of computational resources. Isostrain, isostress and self-consistent interaction models are examples of 1-site models.

Isostrain and isostress interactions present limiting (extreme) cases for the calculated moduli of the aggregate. Self-consistent models, on the other hand, use Eshelby formalism as a basis. It considers a representative sample of the constituents, and computes the polycrystal response as the average of all individual grains (HEM). With the Eshelby's ellipsoidal inclusion theory [9], every grain is approximated as ellipsoidal domains interaction with an infinite domain (HEM) that has the averaged properties of all crystallites. The fact that each crystallite contributes to HEM that interacts with, leads to the term "self-consistent".

Primary aim of all polycrystal plasticity models is to relate macroscopic and microscopic quantities. Unlike the direct geometric modeling of FEM, 1-site models have no or little capacity to account for specific morphological features. A system without pronounced morphological features can be exemplified with an aggregate of randomly-oriented equiaxed grains. Conversely, consider a two-phase (Cu-Nb) multilayered structure where {111} planes of Cu grains and {110} planes of Niobium are aligned normal to the deposition axis of a thin film [10-12]. The mechanical behavior of this material is heavily affected by its structure in comparison to a random organization of grains. While 1-site models have difficulty in implementing the ensuing systematic interaction, it would be valuable to extend the application of these inexpensive models to such cases.

The purpose of this thesis is to investigate the success of the limited tools of 1-site models in representing the mechanical behavior of single and multi-phase systems of prominent morphological features. The thesis will be constrained to the assumption of a single HEM even for multi-phase materials. For this an object-oriented, adaptable software framework will be devised that clearly divides the boundaries of interaction and constitutive models for complete interchangeability. The apparent lack of a software package with these specifics and multi-material capability has been part of the motivation in producing this framework.

1.2. Mesoscale Modeling of Polycrystalline Materials

A polycrystal consists of a large number of single crystals with different orientations that are called grains (or crystallites). Grains of different orientations respond differently to mechanical loading due to the inherent elastic-plastic anisotropy in materials. The properties of the overall polycrystalline solid are consequently dependent on the crystallographic texture, which is the distribution of how the grains are oriented. Mesoscale modeling relates the macro-mechanical behaviors to the micro-mechanical behaviors. The mechanical behavior of the polycrystals has been postulated mathematically at differencing levels of complexity. The material constants in these theories are determined via experiments as pointed out by Bishop & Hill [13]. Mesoscale modeling of polycrystalline materials can be categorized depending on the grain and its interactions with neighbors as 1-site and n-site models. In developing more realistic and complicated theories for polycrystal behavior, two main routes have been followed. The first is the 1-site models such as the isostress and isostrain models in addition to the self-consistent model that this thesis will consider. The second is the *n*-site models mostly using the finite element model (FEM) to physically mimic the polycrystal and the grains that constitute it in the analysis domain.

1.2.1. Point (1-site) Models

1-site models assume that there is only one type of interaction within the polycrystal. If interaction is isostrain or isostress, whole grains inside the polycrystal behave on the same strain or stress state. If the interaction is Eshelby interaction, the elastic-plastic interaction is only in between crystallite and the homogenous medium which is the aggregate of all crystallites.

1.2.1.1. IsoStress & IsoStrain Models. The earliest studies were conducted by Sachs(1928)/Reuss(1929) and Taylor(1938)/Voigt(1938) that are the simplest models of the field. Sachs assumed the stress state is the same for each grain in the polycrystal. This assumption, as a matter of fact, violates the compatibility condition. Conversely, in the Taylor's model, strain state is assumed equal over all crystallites, this time violating the

equilibrium condition. Although these models are not realistic, they gave an idea about the upper and lower bounds for the stiffnesses of the polycrystals. Since these models do not fulfill all the requirements, and the resulting stiffness tensors are the soft and extremes, Hill proposed taking the arithmetic average of isostrain and isostress stiffness tensors to approximate the actual stiffness of the aggregate.

1.2.1.2. Self Consistent Models. Improving on the Taylor and Sachs models, the "self-consistent model" meets the requirements of compatibility and equilibrium and is first proposed by Kroner (1958,1961) [14] and extended by Budiansky and Wu(1962) [15] assuming grains have the same stiffnesses with the average elastic properties of the aggregate. In their models, the relation between stress and strain is found by assuming an elastic-plastic grain inserted as an inclusion into an infinite elastic medium that is representative of the overall crystal, called the homogeneous equivalent medium (HEM). The solution is implemented with the Eshelby [9] elliptical inclusion theorem where each grain is inserted into HEM in succession as shown in Figure 1.1. Hill(1965) [16] extended and introduced the constraint tensor to the single-crystal to find the relation between the elastic-plastic polycrystal and the single-crystal. Lin(1966) [17] established the use of equivalent body-force and employed Green function. In turn, Hutchinson (1970) [6] compared Lin's, Wu's and Hill's methods and applied the spherical grain inclusion to 2-phase FCC composites.

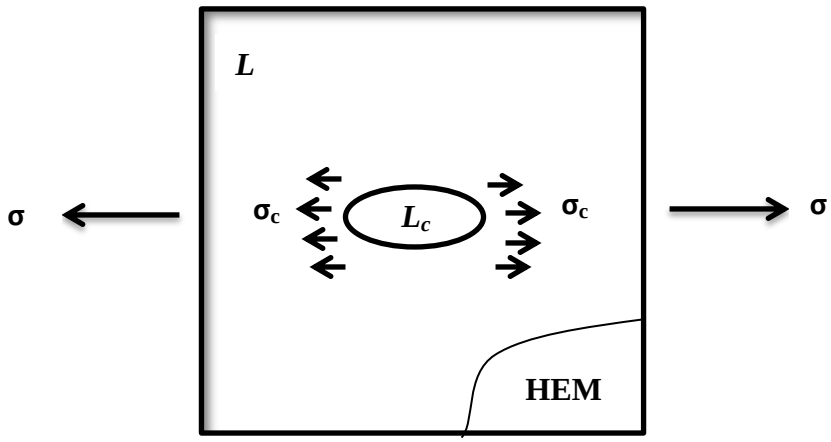

Figure 1.1. Schematic of Eshelby's ellipsoidal inclusion in 2D.

Self-consistent model is a variation over the inhomogeneity problem where the overall domain is assumed to be an aggregate of inhomogeneities. In this case, self-consistent approach proposes that average response of the material has to be same as the overall response of homogenous equivalent medium. The term self-consistent is used because the assumed HEM has to be the averages of the inhomogeneities. Since the interaction between a grain and the average of all grains is considered, this model is completely insensitive to the particular neighbors of a grain (effect of first neighbors). Only the stiffness of the actual inhomogeneity (C_I) is significant, which for a crystalline material depends on the grain's orientation. As a consequence, the self-consistent framework is statistical, in the sense that a given orientation represents all the grains with the same orientation, and the HEM represents the average neighborhood of such set of grains. Also notice, the location of the grains inside the polycrystal cannot be accounted for, since after all Eshelby model considers inclusions in an inifinite medium. When adjacent orientations are correlated or the discontinuity in the physical properties of the neighborhood grains is high, HEM assumption will not be successful in explaining their interactions [18]. These points of breakage for the model are the actual motivations for this thesis. The question is whether the model can be made to or tricked into accounting for such cases.

The two main types of self-consistent polycrystal deformation models are the elasto-plastic (EPSC) and visco-plastic (VPSC) self-consistent models [6,14,16,19,20]. The

EPSC models are used for modeling small deformations; they do not take into account the lattice rotations with plastic slip and they are based on small strain theory [5]. EPSC does not consider grain reorientation, an ongoing process that becomes significant at large deformations. Since a considerable amount of engineering applications do not pose such large deformations, EPSC model is a valuable tool.

In some cases viscosity effects become more important and a rate sensitive method is needed to be considered. At that point model requires a development. Again using the same arguments VPSC model is developed. The VPSC models are applicable to large strain deformation where the elastic properties of the materials are negligible as they are solely based on the plastic deformation of the material. They sometimes considered as rigid plastic which totally ignores the elastic regime. This makes the VPSC models ideal for predicting the material properties after forming processes such as extrusion. In the VPSC models, texture is not just an input as in EPSC, the reorientation of grains is actually an unknown that is tracked [5].

1.2.2. n-site Models

n-site models include FEM(Finite Element Method) and specific versions of point models that have a limited notion of neighborhood effects. In polycrystalline FEM, each grain is composed of a certain number of finite elements which are put together to form the polycrystalline aggregate. Directly simulating the structure of the real crystal, the FEM grain's behavior will be affected by its actual neighbors in addition to its orientation (see Tome *et al*.[21]).

Below, before detailing finite element method, two n-site methods that are extensions of point models are sited.

1.2.2.1. Double Inclusion Model. Double inclusion model is a 2-site point model where each site corresponds to a phase. Lebensohn and Canova [5] used the double inclusion method and showed how the SCM (Self-Consistent Method) can be used in 2 phase materials that contain highly correlated phases. This method is an extended version of

Eshelby and Hill's approach. Each inclusion corresponds to the different phases and these ellipsoidal inclusions *interact* with each other. If a single inclusion is considered, only one Eshelby tensor is utilized whereas one tensor each is required for two inclusions to depict their interaction with the matrix. Furthermore, to account for the direct interaction of the two inclusions, two more Eshelby tensors are added representing the effect of site 2 on site 1 or vice versa [5].

1.2.2.2. Inclusion in Inclusion Model. In another study on extending point models to hierarchical structures, Nemat-Nasser and Hori proposed another multiple inclusion model (1993). They consider modeling an inclusion which contains another inclusion in it. This idea can be extended to more than two phases and the multi-phase material's inclusions are shown in Figure 1.2.

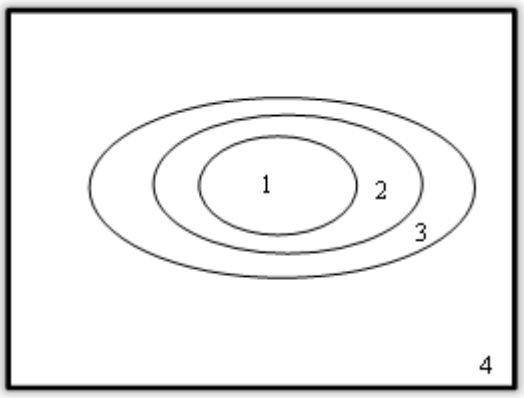

Figure 1.2. Multi-inclusion scheme in a multi-phase material.

The model assumes elastic behavior for all phases. The model provides flexibility by allowing different estimates depending on the combined choice of the outer geometry of the double inclusion and the reference medium. The overall moduli obtained by means of the double-inclusion method, depend on the location and orientation of the inner inclusion, relative to the outer one. Bounds for these moduli can be computed by applying the *universal inequalities,* reported by Nemat-Nasser and Hori [19].

1.2.2.3. Finite Element Method. Polycrystal plasticity and FEM is combined to simulate the deformation of the bodies. FEM has the capability of modeling the deformation much

reliably since it accounts the orientation and neighborhood relations. Although this is the advantage of the FEM to self-consistent model that can only account for the effect of the orientation, FEM has its own complexities such as correct modeling of grain boundary slip. Furthermore, it is very time consuming. The direct comparison with an experiment is also rarely possible since grains inside a polycrystal cannot be mapped or analyzed exactly. Hence, the individual results of FEM can hardly be put to use to understand the material better. If the experiment provides average responses (such as neutron diffraction results of [10,11,20,22-24]), the self-consistent model is still a very effective tool for polycrystal modeling. Due to this, throughout this thesis the alternative models are going to be considered.

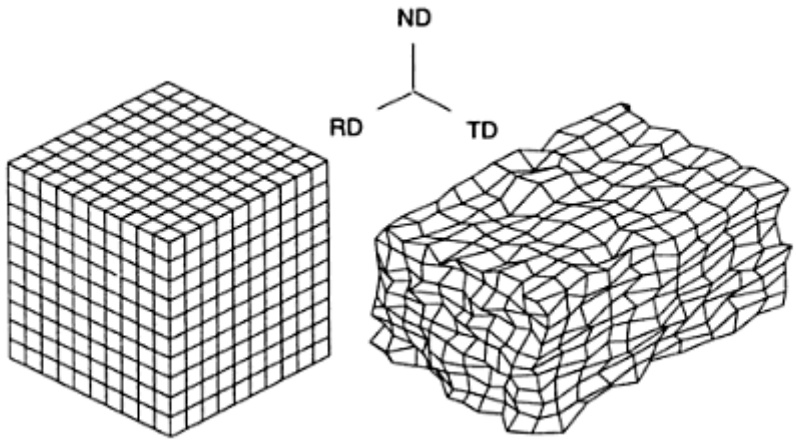

Figure 1.3. A representative FEM simulation[21].

1.3. Morphology / Structural Features

Morphology/structure of a material refers to the *geometric organization* of the constituents of the material in a way that affects the properties. Some of the meso/micro-scale structures commonly observed in engineering materials are sketched in Figure 1.4, in parts a to i. Figure 1.4a shows a single-phase material with equiaxed grains, such as a material after a random solidification process. Figure 1.4b shows a material with needle like grains (elongated along one axis) such as that would be obtained after an extrusion process. Figure 1.4c shows disc-shaped grains whose two in-plane dimensions are large

compared to the third direction. In addition to the geometry of the constituents, number of phases and their relative organization is an important feature of the material structure. Accordingly, following the single-phase examples in Figure 1.4a-c, parts d-i present two-phase structures. Figure 1.4d-f show (i) equiaxed, randomly distributed grains of both phases, (ii) needle shaped grains of one phase in an equiaxed matrix of the other, (iii) alternating layer-shaped grains of two phases, respectively. The latter is commonly observed in vapor-deposited thin films [11]. A structure with particles of one phase that precipitated inside the grains of the other is shown in Figure 1.4g. This structure is commonly observed in precipitation-hardened alloys such as Aluminum alloy 6061 [25] Figure 1.4i shows randomly-oriented needle-like grains of one phase inside a matrix of another. This can be exemplified with a typical short-fibre composite. Finally, Figure 1.4h represents a material where grains are made up of alternating layers of two phases. For example, $(\alpha + \beta)$ Ti alloys exhibit this morphology with the hexagonal-close-packed (HCP) α phase and the face-centered-cubic (FCC) β phase.

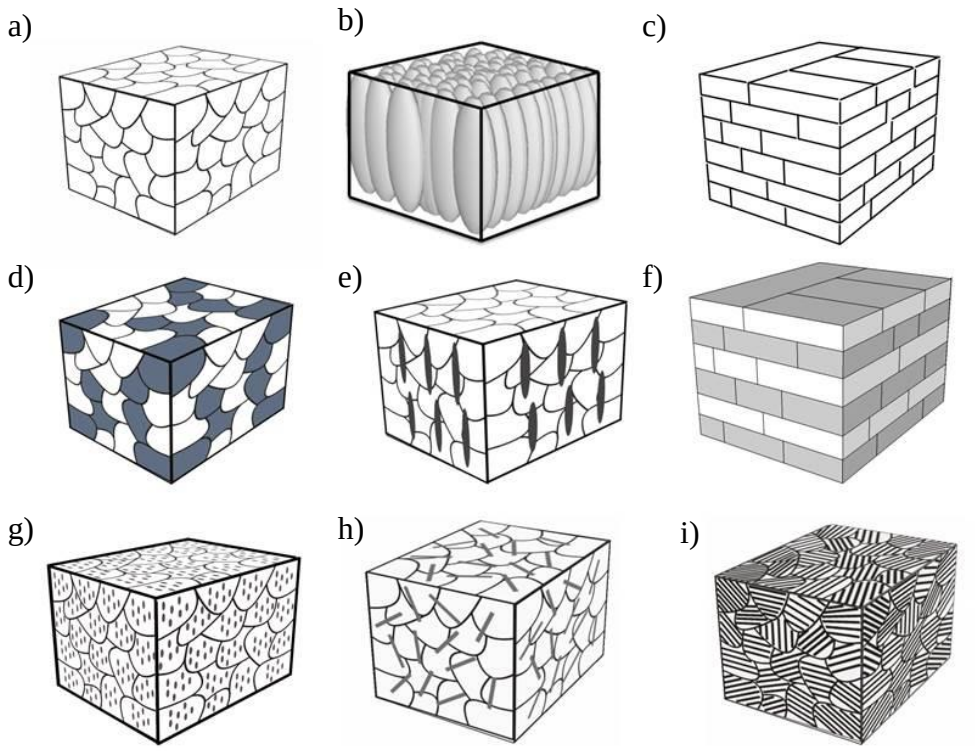

Figure 1.4. Classification of microstructures. single-phase: (a) equiaxed grains, (b) fiber grains, (c) lamellar grains; multi-phase: (d) equiaxed grains, (e) oriented fibers inside an equiaxed grain matrix, (f) multi-layer, (g) dispersions inside a matrix, (h) short fiber reinforced matrix, (i) correlated, two-phase layered structure.

An additional structural feature that is not visible in Figure 1.4 is the orientation distribution of the grains that make up a polycrystal. This is called the crystallographic texture. Extruded structures as in Figure 1.4b and deposited structures Figure 1.4f exhibit strong textures whereas lack of any preferred orientation (e.g., an as-cast material) is named “random texture”.

In two phase materials, correlations between the orientations of neighboring constituents may also be important. Such correlation is not presented by the texture information of individual phases. For example, correlation exists when two regions of adjacent phases are layers and their relative crystallographic orientations are subjected to

the Burgers relation [7]. α and β phases inside a Ti-Al alloy exhibit correlation when these phases have lamellar structures (see Figure 1.4i). In this case, the specific correlation between crystallographic planes/directions of the neighboring α and β phases are given by: $\{10\bar{1}0\}_\alpha // \{112\}_\beta$ and $\langle 1\bar{2}10\rangle_\alpha // \langle 111\rangle_\beta$

FEM has the capability of considering the shape and structure of the grains by direct geometric modeling. So, any structure in Figure 1.4 can, in principle, be modeled by FEM though computation costs will be excessive. On the other hand, point models usually have limited ability to take shape effects into account – though accounting for texture is usually possible. Morphological parameters do not exist at all in primitive point models like isostrain and isostress models (Section 1.2.1.1). On the other hand, SCM (Section 1.2.1.2) using Eshelby interaction allows a limited adjustment for morphological effects, through varying the dimensions of the Eshelby ellipsoid. In particular, this allows representing fiber-like and layer-like grains (structures) in addition to equiaxed grains by adjusting the ellipsoid radii accordingly. Through utilization of the 2-site double-inclusion model (Section 1.2.2.1), correlated orientations in multi-phase materials can also be modeled.

To detail the morphological tools of SCM models further, categorize them as “single phase” and “multi-phase”. Single-phase micro-structures that SCM can represent include equiaxed grains, lamellar grains and fiber-like grains (Figure 1.4a-c). It is evident that grain morphology would affect the mechanical response of the material. Single-phase polycrystals, where the dominant microstructural parameter is the shape of the grain, can be best modeled when the limit of the shape used in the SC goes to the shape of the grain. Since the Eshelby inclusions are ellipsoidal, playing with the dimensions of the radii gives the geometry of the microstructure. If the axes of the ellipsoid are (a, b, c) then the comparison of the radii can be expressed with using notation as, equiaxed grain a=b=c, lamellar grains $a = b \gg c$ and fiber grains $a = b \ll c$. Figure 1.4 represents the possible microstructures that SCM can predict the response when the appropriate corresponding inclusion form is found in Figure 1.5. Basic 3 shapes of inclusion that can define the morphologies for the polycrystals are shown in the Figure2a, b, c. With appropriate combination of these 3 shapes a considerable part of the grain morphologies can be modeled.

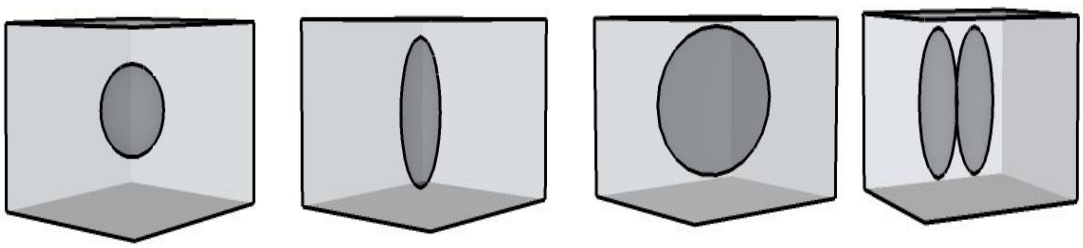

Figure 1.5. Eshelby ellipsoids with different aspect ratios. (a) spherical inclusion, (b) needle-like inclusion, (c) disc-shaped inclusion, (d) double-inclusion.

Although ellipsoidal inclusion concept is part of the Eshelby interaction, results of the SCM can reveal the isostrain and isostress behaviors of polycrystal. Isostrain behavior means that response of the polycrystal is such that grains have the same strain state independent of orientations. If the inclusion has a shape of a needle, SCM using Eshelby interaction gives the strain response of the polycrystal same as isostrain interaction. Above statement is valid also for isostress. If the inclusion has a shape of disc, SCM using Eshelby interaction gives the stress response of the polycrystal same as isostress interaction. These are going to be explained in detail in the Discussion part.

Straightforward SC modeling has particular difficulty in representing some multi-phase structures. Consider a two-phase aggregate (i) composed of equiaxed grains, (ii) composed of planar grains in a layered arrangement, (iii) needle-shaped grains of one phase in a matrix of the second phase. The difference in structure in all these cases will obviously create a difference in the mechanical behavior. Self-consistent model has actually success in representing the effect of these morphologies, because of the similarity of the constituents to ellipsoids. Some examples used in the literature for the multi-phase structures are stated below.

A two phase FCC composite of equiaxed grains is considered by Hutchinson[6] as in Figure 1.4d. In that article, a spheroidal grain inclusion is placed inside a homogeneous medium and a macroscopic stress is applied on this medium. Stress in each grain is calculated individually. The macroscopic moduli are given as the appropriate averages of the properties of the grains. Corresponding elliptic shape is schematically shown in Figure

1.5a. Above procedure is conducted for both of the phases: interaction of spheroidal grain of phase1 with the medium and the interaction of spheroidal grain of phase2 are taken into account and a meaningful overall stiffness value is found. Spherical inclusion is chosen because it is the best morphology to reflect the mechanical response.

Another case is columnar grain case, which can be represented by disc-shaped ellipsoids as in Figure 1.4f. Model can be achieved by introducing two different phases with the same morphology. Both phases are individually plugged inside the HEM with considering morphologies as in Figure 1.5c. The columnar grain of alternating layer morphology as stated before is a challenging issue for the routine self-consistent model when a certain correlation in between two phases exists as in Figure 1.4h. Manipulation of the immediate model only by changing the axis length of the elliptical inclusion is not enough. Therefore, further manipulations are required concerning the relations between two phases. Examples of this kind are martensitic stainless steel, Ti-Al alloys and Cu-Nb alloys with strong morphologies. In the article of G.R.Canova [7] correlation in Ti-Al alloy is considered and a 2 site model is developed to reach the desired morphology. 2 site-models can have different possible morphological representations but for the specific example two tangent inclusions inside a medium is enough as Figure 1.5d.

Short-fiber composites are the particular case for polycrystalline materials consisting of a matrix reinforced by a dispersed phase in the form of discontinuous fibers like reinforced SiC/Al composites. In the morphological representation of fibers, a needle-like inclusion is enough to give the effect of the shape of the grains to the interaction. Representation of the matrix is organized with spherical inclusions as indicated schematically in Figure 1.4e.

Another form that SC cannot represent is the hierarchic modeling. To exemplify consider the case where the precipitates inherent inside a matrix as in Figure 1.4g. Precipitate defined as a different phase inside a solid. Materials including precipitates are classified according to the location of the precipitates inside the material. When they are positioned inside a grain as in Figure 1.4g, they exhibit different behavior from the matrix material due to their structural and elastic properties. Such a case is versatile to a

hierarchic modeling since at the lowest level precipitates and the matrix accommodate to a grain and each grain constitutes the higher-level material. Hence, there are HEMs inside HEM. Self-consistent modeling will offer solution to this kind of morphology after manipulating the immediate codes. Using this kind of modeling will serve a solution to Al-Al_2O_3 or different materials including precipitates inside the grains.

Although SC includes many morphologies, it cannot model the certain cases such as fiber structures having different angle of orientations as in the Figure 1.4h. Axes of the ellipsoid have to be perpendicular or parallel to the sample coordinate system axes. But there are bunch of cases that the fibers are not aligned with the sample coordinate system axes. For example, consider the case where the fibers oriented 45^o to the right on the xy plane and on top of it another layer of fiber oriented 45^o to the left and periodically repeats. Routine self-consistent model uses a strict orientation that allows only 3 kinds of morphologies. But infusion of the eshelby inclusions rotation freely on around any axes lets to model the grain orientations. The defeated problems and example cases will be discussed further in the discussion part.

1.4. Scope

This thesis primarily investigates the tools and model adaptations to make self-consistent models capable of modeling a limited set of structural features in multi-phase materials. To this end, a Python® based flexible code structure is generated that can accommodate the current applications in the literature and possible other improvements. This structure will be called Adaptable Point Model Framework (APMF). These models are compared by their applications to several test cases inspired from Figure 1.4.

Ellipsoidal grains with large aspect ratio's (e.g., columnar grains) where the grains are arbitrarily oriented with respect to the sample coordinate system cannot be modeled with the current implementations of the self-consistent method. Similarly, multi-phase aggregates are not usually supported. These are not impossible by principle; but rather require more extensive numerical implementation. One of the aims is infusing morphology to the immediate point (1-site) models in order to make them more useful. Successful

meso-scale modeling of structures with pronounced morphology would allow avoiding the more expensive and complicated FEM models.

APMF is developed with multi-phase capability and such that morphological parameters of each grain can be introduced independently. To test the framework and investigating the ability to model multi-phase aggregate of pronounced morphological structure, Copper and Niobium aggregate are considered. This choice is inspired from multilayered structures [10,12] of these materials. An additional factor in this choice is the highly anisotropic nature of both Copper and Niobium. High anisotropy leads to highly heterogeneous stress/strain fields within the aggregate and creates a better test from meso-scale models.

Software abilities are used efficiently. As the results contain enormous amount of information, it is necessary to use an effective storage tool. Hence, APMF will employ a flexible data base structure. Further properties of APMF are introduced in Chapter 3.

2. THEORY

2.1. Crystallographic Texture

It is a well-known fact that macro-behavior of a material depends on the microstructure. Microstructure of a material is defined by the orientation of the constituents. Texture is the distribution of the orientations inside an aggregate. It is mostly used as the "preferred orientation" in the literature. However, a random orientation also considered as a texture. Throughout this thesis the word texture is used in the meaning of a non-uniform distribution of crystallographic orientations in a polycrystalline but if there is an adjective before the word texture like: *random* texture, focus is on the adjective part.

A single crystal has an orientation scheme that is all of the crystallites are looking to the same direction; a random texture has the crystallites where each orientation is present inside the aggregate. In between 2 extremes, a group of the crystallites will be oriented in the same direction or a group of orientation has *preferred* by the polycrystal. This *preferred* orientation scheme can be formed by some mechanical processes or during manufacturing. Deformation of the material displays on the macrostructure which is determined by the microstructure. Texture and non-texture models can be classified according to the requirements. (i) Orientations inside a sample is determined by diffraction tools. To detect the orientations of the constituents inside the polycrystal, some methods are developed such as X-ray, neutron, electron-back scattering methods. These methods are based on the diffraction techniques. By using a proper method textured sheet metals configurations can be detected. (ii) A new orientation distribution is generated such that overall behavior of the aggregate as same as the sample. If a Copper $\langle 111 \rangle$ texture is the need, then an orientation scheme is generated such that $\langle 111 \rangle$ grains are occupying a significant place. Both of these techniques can be used to give a foresight for the response of the aggregate.

Textures that have been mostly investigated in the metallurgy have been those in rolled sheets of materials of cubic lattice structure [21]. Representation of the texture is

as $\{h\ k\ l\}\ \langle u\ v\ w\rangle$, where $\{h\ k\ l\}$ represents the planes of that family parallel to the plane of the rolled sheet (aligned with the ND (normal direction)) and $\langle u\ v\ w\rangle$ represents the direction on the $\{h\ k\ l\}$ plane aligned with the RD (rolling direction). For instance, $\{2\ 1\ 1\}\ \langle 1\ 1\ 1\rangle$ means $\{2\ 1\ 1\}$ family of planes are parallel to the sheet plane and their $\langle 1\ 1\ 1\rangle$ directions are aligned with the rolling direction.

Materials having each kind of orientation in equal amount or the materials whose distribution frequency is equal, called as isotropic materials. In all directions there exists at least a member of $\{h\ k\ l\}$ plane family which means material is independent from directions having the same properties. A special case of isotropy is the transverse isotropy. Material is highly textured along a direction and perpendicular to that direction a plane exists. Crystal planes which are parallel to that plane establish a uniform distribution. As a result perpendicular to the textured direction, every direction has the same physical properties. Materials having this kind of orientation distribution are called transversely isotropic materials.

The degree of the texture can be measured with different indicators. One of these is the anisotropy ratio. Anisotropy ratio is defined as :

$$AR = \frac{2c_{44}}{c_{11} - c_{12}}, \qquad or \quad AR = \frac{2(s_{11} - s_{12})}{s_{44}}. \tag{2.1}$$

Where AR is the anisotropy ratio and c_{ij}, s_{ij} are the stiffness and compliance matrix, respectively. Physical meaning of the AR is that it characterizes the relative response of cubic crystals to two different types of shear strain: c_{44} reflects the behavior of the shear strain response on $\{1\ 0\ 0\}$ planes $\langle 1\ 0\ 0\rangle$ directions and $c_{11} - c_{12}$ reflects the behavior of the shear strain response on $\{1\ 1\ 0\}$ planes $\langle \bar{1}\ 1\ 0\rangle$ directions.

Another texture degree measurement technique is: considering the maximum and minimum values of the effective elastic modulus, from among all possible line orientatitons in a cubic crystal, where found to exist for orientations along the [1 0 0] and [1 1 1] directions.

$$\frac{1}{E_{hkl}} = \frac{\varepsilon_{hkl}}{\sigma_{hkl}} = s_{11} + \frac{(2s_{12} - 2s_{11} + s_{44}).(k^2l^2 + l^2h^2 + k^2h^2)}{(k^2 + l^2 + h^2)^2} \quad (2.2)$$

E_{hkl} is the directional Elastic modulus along hkl. Extreme values are

$$E_{100} = \frac{1}{s_{11}}, \qquad E_{111} = \frac{3}{s_{11} + 2s_{12} + s_{44}}, \frac{E_{111}}{E_{100}} = \frac{3s_{11}}{s_{11} + 2s_{12} + s_{44}}, \quad (2.3)$$

[1 0 0] direction is the softest and [1 1 1] direction is the stiffest direction in some cubics (Al, Cu, Si, Fe and Ni) and reverse is true for Nb, Cr and Mo [22]. The 3rd ratio in Equation 2.3 is a representation of anisotropy ratio for cubic materials. The modulus in Equation 2.2 can be expressed in terms of maximum and minimum values: E_{111} , E_{100}.

$$\frac{1}{E_{hkl}} = \left[\frac{1}{E_{100}}\right] + \left\{\frac{3(k^2l^2 + l^2h^2 + k^2h^2)}{(k^2 + l^2 + h^2)^2}\left[\frac{1}{E_{111}} - \frac{1}{E_{100}}\right]\right\} \quad (2.4)$$

2.1.1. Orientation

As stated above, orientation of grains has major effects on the macro-behavior of the polycrystalline materials. Since each direction on a crystalline structure, most of the time, has different elastic properties, total aggregate depends on the arrangement of the orientations. An FCC cubic lattice has the stiffest direction mostly in ⟨1 1 1⟩ directions due to the close-packed structure of the FCC. For a directionally solidified perfect single crystal or a fiber whose crystallographic {1 1 1} s are oriented with the sample ⟨1 0 0⟩ direction exhibits the same elastic stiffness with the crystal stiffness along that direction. Hence, polycrystalline sample deforms less along that direction.

As can be realized, spatial distribution of the orientations affects the total behavior of the material. Determination of how much from an orientation of grains occurs inside an aggregate is critical for the modeling. Data coming from the source should be adjusted for analytical models due to having noises in data or just for mathematical purposes. Since data is containing only discrete values of orientation scheme, taking a crystallite orientation distribution function (ODF), which describes the frequency of existence of

specific orientations in a three-dimensional orientation space, eases the calculations. This space is usually defined by three Euler angles which is constituted from a set of three successive rotations. One kind of Eulerian representation of the orientation is using the Bunge angles. These angles correspond to three successive rotation operations to bring the crystal coordinate system into coincidence with the sample coordinate system.

An orientation can be described by three parameters and denoted as g. Eulerian space consists of many$g$'s which are relating the sample coordinate system (S) to crystal coordinate system (C). From a given S with coordinate axes: (x, y, z), rotations performed consecutively as:

(i) Rotate around z with an angle φ_1, $0 < \varphi_1 < 2\pi$
(ii) Rotate around x with an angle ϕ, $0 < \phi < \pi$
(iii) Rotate around again z with an angle φ_2, $0 < \varphi_2 < 2\pi$

The complete ODF consists of the sets of g's such that all the crystallites in the specimen is characterized and a continuous feature is attained. Continuous feature of ODF enables the use of texture modeling [18].

2.1.2. Diffraction

Diffraction is a method to measure the texture of a polycrystalline material. Historically, most of the knowledge about the atomic arrangement in solids has resulted from the diffraction techniques. Diffraction occurs when a wave face with obstacles that are capable of scattering the wave, and have space that are comparable in magnitude to the wavelength that constructively interferes [26]. As in Figure 2.1, an incident beam strikes to the sample and reflected particles are detected by point detectors or area detectors. According to the reflection angle using Bragg's law the crystallite orientations can be determined.

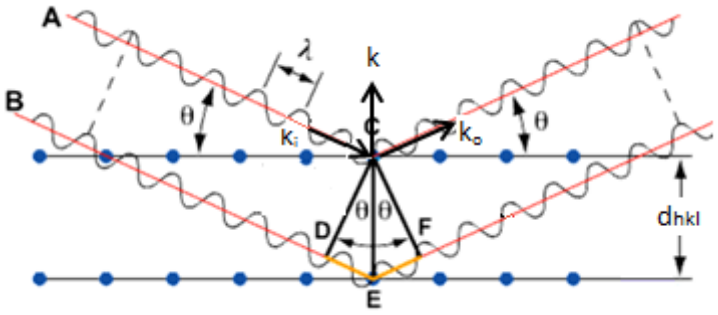

Figure 2.1. λ is wavelength of the monochromatic x-rays, d is the lattice interplanar spacing of the crystal, θ is the X-ray incident angle that provides constructive interference, ki is the direction of the incident beam, ko is the direction of reflected beam, k is the normal of the plane.

Consider two planes that are parallel to each other. Spacing in between these planes is d_{hkl}(Lattice distance) where hkl is the representation of the crystallographic plane. Relation in between the diffracted beam and the angle of the incident beam is determined by the Bragg law. That asserts: If the wave length of the incident beam is appropriate for the lattice distance, a diffraction of the 2 rays or more can be detected by the detectors. Difference of the paths that is travelled by the 2 rays must be equal to an integer in order to a complete constructive interference. Using this phenomenon, relation becomes in the form of:

$$\lambda = 2d_{hkl} \sin\theta \tag{2.5}$$

where θ is the angle of the incident beam with the surface of the material and λ is the wave length. Direction of the incident beam and the unit length is vectorized by $\vec{k}_i$ and reflected beam is $\vec{k}_o$. Normal of the plane indicates the planes where the angle θ and atomic lattice distance matches. Normal of the plane can be expressed mathematically by the vector $\vec{k}$. $\vec{k}$ is a unit vector that is enough to describe the planes of the specific θ.

$$\vec{k} = \frac{\vec{k}_o - \vec{k}_i}{\left\|\vec{k}_o - \vec{k}_i\right\|} \tag{2.6}$$

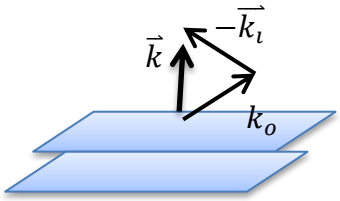

Figure 2.2. Schematic of diffraction geometry.

Although some diffraction techniques employ some special case of x-ray and neutron techniques, Bragg's law is valid for these cases since there is always a diffraction measurement. Placed detectors encounter with some peaks in some angle θs. At those points planes of interests are identified and according to their intensities, their volume fraction inside the specimen can be calculated.

2.2. Constitutive Models

Point models are the models that couple the constitutive and interaction models. The former one relates the plasticity, latter relate the interaction type (Eshelby, isostrain, etc.) with the stiffness. Nature of the problem allows to a complete separation of the constitutive and interaction parts. This section declares the slip plasticity and the hardening law of the constitutive models.

2.2.1. Slip Plasticity

Plastic deformation is the permanent deformation of a crystallite which occurs in two steps. Firstly, lattice is distorted elastically until the yielding point is reached. After the yielding point, plastic activity begins due to slip or twinning. Since the focus of this thesis is on the slip activity of crystals, twinning deformation is considered as a future work.

Slip plasticity is physically manifested by the movement of crystal line defects called dislocations. Dislocations can move on, in response to shear stresses, only in certain crystal planes in certain crystallographic directions due to their energetics. In a single crystal, slip occurs on crystallographic planes with the highest resolved shear stress. The preferred plane and direction pair is called a slip system (e.g. 12 easy slip systems in face centered cubic crystals). The slip system that exhibits plastic slip under a given loading is the one that has the highest resolved shear stress.

At the atomic scale, slip occurs on the densest atomic planes and direction has the highest linear density in order to minimize the distortion during motion [26]. Possible slip systems for different atomic packing structure are tabulated in Figure 2.1. [24]. Considering an FCC unit cell; the most closely packed plane is the $\{1\ 1\ 1\}$ plane family and on this plane the highest density is along $\langle 1\ \bar{1}\ 0 \rangle$ directions. There is more than one direction on a plane that provides the requirements. Therefore, 4 planes and 3 possible directions for each plane yields 12 slip systems that can be activated inside an FCC crystal. In Table 2.2 all family members of the FCC possible slip systems are tabulated.

Table 2.1. Slip systems for face-centered cubic, body-centered cubic and hexagonal close-packed crystals.

Slip Plane	Slip Direction	Number of Slip Systems
FCC		
$\{1\ 1\ 1\}$	$< 1\bar{1}0 >$	12
BCC		
$\{1\ 1\ 0\}$	$< \bar{1}\ 1\ 1 >$	12
$\{2\ 1\ 1\}$	$< \bar{1}\ 1\ 1 >$	12
$\{3\ 2\ 1\}$	$< \bar{1}\ 1\ 1 >$	24
Hexagonal Close-Packed		
$\{0\ 0\ 0\ 1\}$	$< 1\ 1\ \bar{2}\ 0 >$	3
$\{1\ 0\ \bar{1}\ 0\}$	$< 1\ 1\ \bar{2}\ 0 >$	3
$\{1\ 0\ \bar{1}\ 1\}$	$< 1\ 1\ \bar{2}\ 0 >$	6

All of these systems are not activated under a given straining condition, since activation requires exceeding the critical level for shear stress. Which system is active is determined by the resolved component of the stress on the plane of the slip systems.

Table 2.2. 12 Slip systems belongs to {1 1 1} <110> family set.

(1 1 1)			($\bar{1}$ 1 1)			(1 $\bar{1}$ 1)			(1 1 $\bar{1}$)		
[$\bar{1}$ 1 0]	[$\bar{1}$ 0 1]	[0 1 $\bar{1}$]	[1 1 0]	[1 0 1]	[0 $\bar{1}$ 1]	[$\bar{1}$ 1 0]	[$\bar{1}$ 0 $\bar{1}$]	[0 1 1]	[1 0 1]	[0 1 1]	[$\bar{1}$ 1 0]

Activation is determined by the ratio of the resolved shear stress to the critical resolved shear stress. Generally, if it is much higher than 1 then the slip mechanism prefers that system. In Figure 2.3 projection of the uni-axial load on a specific plane is represented. Applied load F leads to a stress of σ. Resolved component of σ on the slip plane in the direction of slip can be represented with the Equation 2.9. Where τ_{RSS} is the resolved shear stress on the slip plane and ϕ, λ are the angles in between the tensile axis and the slip plane, slip direction, respectively.

Load projected on the plane λ, has an area of A_λ

$$A_\lambda = A \,/\, \cos\lambda \tag{2.7}$$

where A is the cross-section of the specimen. Component of the F on the inclined λ plane is F_φ.

$$F_\phi = F \cos\phi \tag{2.8}$$

Since the stress occurs on the plane is F/A . The resolved component of the load on the plane is F_φ which is the shear force. Stress effect of this force is F_φ / A_λ .

$$\tau_{RSS} = \sigma \cos\phi \cos\lambda \tag{2.9}$$

Cosine part of the Equation 2.9 expresses the sensation of the shear stress on the slip system *s*. Since a cubic crystal has more than 1 slip system and for complex computations, it is essential to represent these systems with a tensor. Each system can be gathered inside, Schmidt tensor (μ^s), that resolves the load or strain on to the slip system *s*. Equation 2.10 expresses the resolved shear component of the stress or strain on the system *s* where n is the normal of the plane and m is the direction of the slip.

$$\mu^s = \frac{1}{2}(n_i m_j + n_j m_i) \tag{2.10}$$

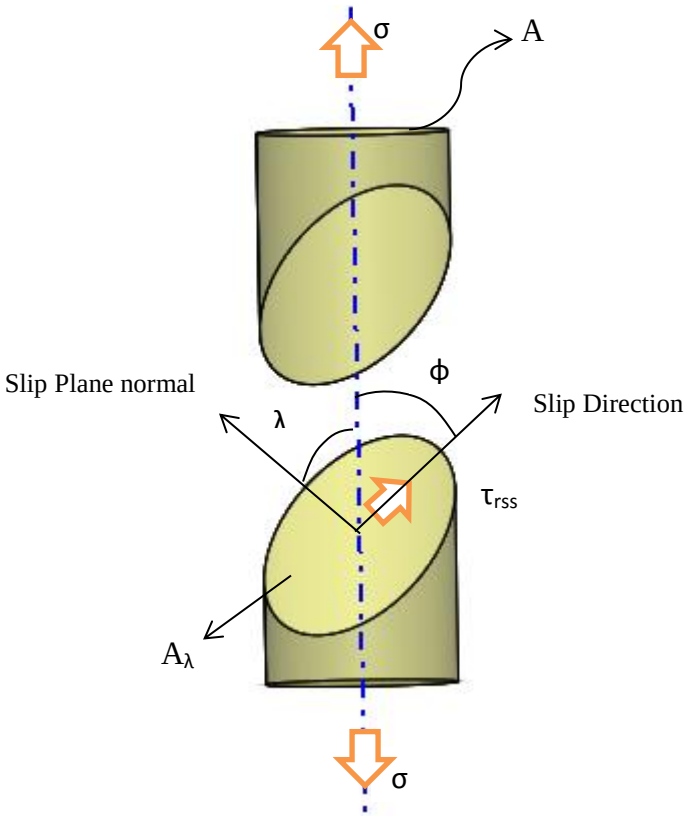

Figure 2.3. Geometrical representation of a single crystal under tensile load.

A stress state in 3D is represented by a 3x3 symmetric matrix, where each component shows the stresses specific to the chosen coordinate system. A 3x3 symmetric stress matrix can be represented by 6 eigentensors of the particular elastic stiffness tensor

of the considered material. These eigentensors hence depend directly on the material's single crystal stiffness and its symmetry level. (For the interpretation of a cubic material's eigentensors, see [18]) The incompressibility condition (preservation of volume) of slip plasticity provides an additional equation on the stress state. This means 5 independent slip systems are needed to yield an arbitrary plastic deformation. Considering the FCC structure there are 12 slip mechanisms with $\{111\}\langle 110\rangle$ slip systems. Given 12>5, there are multiple paths (combinations of slip systems, 96 possible) to generate the same plastic deformation. The physically realized 5 is determined by the theory of *minimum work* postulated by Taylor (1938) [27]. This theory considers the strain energy for each combination and picks the one with the least energy as the selected mechanism for the plastic deformation. Hence,

$$\sum_{\alpha=1}^{n} \tau_c^{\alpha} \dot{\gamma}^{\alpha} \leq \sum_{\alpha=1}^{n} \tau_{c*}^{\alpha} \dot{\gamma}_*^{\alpha} \tag{2.11}$$

where τ_c^{α} is the current shear strength of the α^{th} physically-activated slip system and τ_{c*}^{α} is the current shear strength of the α^{th} geometrically possible slip system. $\dot{\gamma}^{\alpha}$ is the shear strain rate of the α^{th} actual slip system, $\dot{\gamma}_*^{\alpha}$ is the shear strain rate of the α^{th} geometrically possible slip system. It is also known as minimum shear principle since his assumption of isotropic hardening results in the elimination of the shear stress. After using isotropic hardening assumption 2.11 reduces to the comparison of shear rates:

$$\sum_{\alpha=1}^{n} |\dot{\gamma}^{\alpha}| \leq \sum_{\alpha=1}^{n} |\dot{\gamma}_*^{\alpha}| \tag{2.12}$$

Absolute value indicates that reverse shear is considered same as the forward one. Taylor also showed that the $\binom{12}{5}$=792 combinations in FCC are further constrained due to the 3 slip directions in each slip plane being linearly dependent since,

$$a_1 = -\frac{1}{2}(a_2 + a_3) \tag{2.13}$$

where a_1 a_2 and a_3 are the directions on each plane of slip. Consequently, possible number of combinations reduces to 96 in FCCs.

For an FCC crystal if the resolved shear stress on 12 planes is higher than the critical resolved shear stress, plasticity starts. Passing the yield point of the material dislocations pile up and deformation hardens. Three criteria for the yield that is considered are:

$$\begin{gathered} \dot{\gamma} > 0 \\ m^s : \sigma_c = \tau^s \\ m^s : \dot{\sigma}^s = \dot{\tau}^s \end{gathered} \tag{2.14}$$

For a system to slip, it has to be potentially active and remain under load. This means that the stress must originally be on and remain on the yield surface facet corresponding to that system during the incremental step. Hardening character of the material can be modeled with different models. Isotropic, kinematic, Voce Law, Power Law hardening models are the adaptable models for different materials. Since the results are mainly built on the Voce Law , a detailed explanation is needed.

2.2.2. Hardening Laws and Tangent Stiffness

The hardening in SCM in literature generally uses Voce hardening laws. In here, G.I. Taylor's classic isotropic hardening rule (proposed in 1923), which is almost universally adopted in the metallurgical literature for various approximate analyses of single and poly-crystal deformation is used [28].

Hardening can be separated into two parts based on the interaction of slip systems. Latent hardening and self-hardening, where former one represents the propagation of dislocations of one system s to another system s’ and the latter one represents the self-dislocation motion on the system s. Mathematical correspondence of these types are a

hardening coefficient matrix: $h^{ss'}$. h^{ss} is the diagonal elements and values are displaying the degree of the self-hardening and $h^{ss'}$ is the latent hardening where s≠s'. If the difference in between hardening types is indistinguishable then the values of hardening coefficient matrix are equal to one, $h^{ss'}=1$.

2.2.2.1. Voce. Voce type hardening is among the most used hardening types in the literature. It has many kinds like three parameter Voce law, Swift Voce law, generalized Voce law, extended Voce law etc… In this thesis extended Voce law is used just for to choose. Working principle is that critical resolved shear stress develops from the accumulated shears inside the grain. This kind of Voce law has four parameters. Through a curve fitting approach, threshold stress on the system which is a function of the total strain, is as in Equation 2.15.

$$\hat{\tau}^s = \tau_0^s + (\tau_1^s + \theta_1^s \Gamma)\left(1 - exp\left(-\frac{\theta_0^s \Gamma}{\tau_1^s}\right)\right) \tag{2.15}$$

where τ_0^s is the critical resolved shear stress of the s^{th} slip system. $\tau_1^s, \theta_0^s, \theta_1^s$ are the remaining 3 parameters where θ s are the hardening slopes at the beginning and the asymptotic hardening rate, respectively. $\tau_0^s + \tau_1^s$ is the back-extrapolated critical resolved shear stress. $\Gamma = (\sum_s \Delta\gamma^s)$ is the accumulated shear strain inside each grain. These parameters are reflecting a curve fitting procedure.

Change in CRSS can be calculated for a time interval Δt as:

$$\Delta\tau^s = \frac{d\hat{\tau}}{d\Gamma}\sum_{s\prime} h^{ss\prime}\dot{\gamma}^{s\prime}\,\Delta t \tag{2.16}$$

Where critical resolved shear stress rate per accumulated shear strain on the slip system is the Voce function.

$$V^s(\Gamma) = \frac{d\hat{\tau}^s}{d\Gamma} = \theta_1 + (\theta_0 - \theta_1 + \frac{\theta_0\theta_1}{\tau_1}\Gamma)exp(-\frac{\theta_0^s\Gamma}{\tau_1^s}) \tag{2.17}$$

From Equation 2.16 shear stress rate for the critical point is :

$$\dot{\tau}^s = \sum_{s\prime} V^s(\Gamma)h^{ss\prime}\dot{\gamma}^{s\prime} \tag{2.18}$$

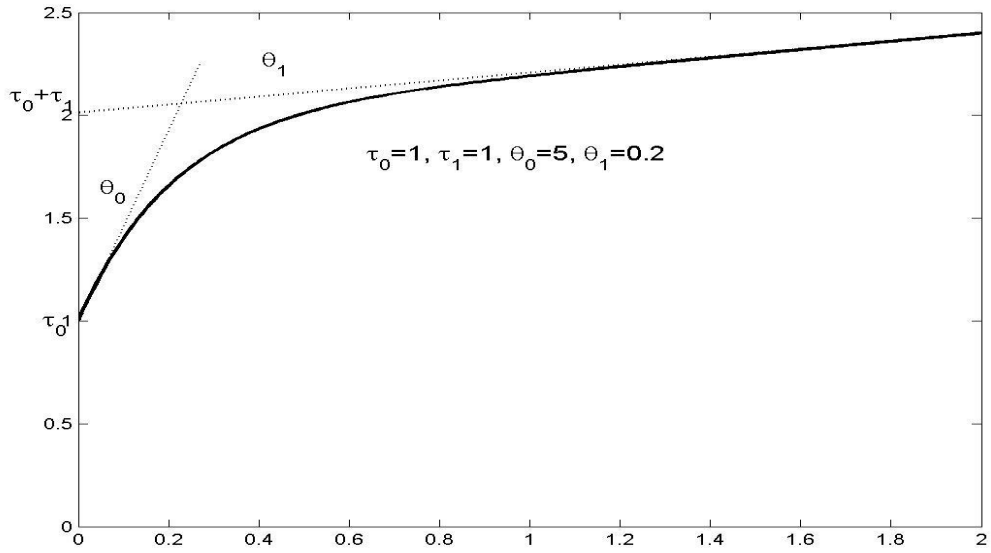

Figure 2.4. Sketch of Voce-type hardening with the model parameters indicated.

Equation 2.18 states the contributions of the deformation history and the current reactions of the slip systems on the hardening. Voce function part is demonstrating the slope of the stress-strain curve which is dependent on the accumulated shear strain and the remaining part is the current deformations effect on the individual slip mechanisms.

Contribution of the hardening to the stiffness matrix is one of the principal requirements to solve the overall behavior of the material. As the load increase single crystal instantaneous stiffness becomes more compliant:

$$L_c = C_c : \left(I - \sum_s \mu^s \otimes f^s \right) \tag{2.19}$$

where C_c is the elastic stiffness of the single crystal and L_c is the tangent stiffness of the single crystal. f^s is the projector tensor which projects the strain rate tensors of the crystal to a shear strain rate for each active slip system :

$$\dot{\gamma}^s = f^s : \dot{\varepsilon}^c \tag{2.20}$$

It is given by

$$f^s = \sum_{s'} (X^{-1})^{ss'} \mu^{s'} : C_c \tag{2.21}$$

Where the sum is over active slip systems and X is given by:

$$X^{ss'} = \mu^{s'} : C_c : \mu^s + V^s(\Gamma) h^{ss'} \tag{2.22}$$

The second term inside the X is related to the hardening law and the first term is coming from the elastic part which remains constant since rotations of the crystals are not considered. Voce part of the equation dependent on the accumulated shear and for isotropic hardening each slip system has to have the same Voce parameters. As a requirement hardening coefficient matrix has to have the same values.

2.3. Interaction Models

A HEM is constituted from grains which have different geometrical and mechanical properties. Since each grain is in the neighborhood of the other grains, they have relations with each other that control the overall behavior of the material. A lattice mismatch between the grains or different slip patterns between grains even having the same mechanical properties for each orientation, affects the mechanical behavior of the

aggregate. A poly-crystal model mimics the ingrain behavior with constitutive part and the relation between the grains is mimicked by the interaction part.

Deformation in polycrystalline materials is complex due to the diverse harmony of crystallographic orientations of the numerous grains; the direction of slip varies from one grain to another. Therefore interaction with its surroundings becomes a fundamental question: how much of the deformation is accommodated by the grain itself and how much is the surrounding grains. Although stress/strain share of grains is the result of this interaction, total weighted averages of them has to be equal to the macroscopic stress/strains. Hill [16] demonstrate that under general conditions the volume averages of the stress and strains for crystallites has to be equal to the overall stress and strain. That is:

$$\varepsilon = \langle \varepsilon_c \rangle = \frac{1}{V} \int \varepsilon_c dV \tag{2.23}$$

$$\sigma = \langle \sigma_c \rangle = \frac{1}{V} \int \sigma_c dV \tag{2.24}$$

For our model, elastic stiffness and the thermal expansion tensors of the crystals C_c, α_c are known. The texture is also known with volume fractions of each orientation. C, α are the overall tensors of the polycrystal. The only assumption that is made is that uniform stress and strain inside the grains. If the polycrystal subjects to an incremental temperature change δT and uniform stress and strain, strain of the crystal can be represented like:

$$\varepsilon_c = C_c^{-1} : \sigma_c + \alpha_c \delta T \tag{2.25}$$

Using 2.23, overall strain can be calculated as:

$$\varepsilon = \langle \varepsilon_c \rangle = \langle C_c^{-1} : \sigma_c \rangle + \langle \alpha_c \rangle \delta T \tag{2.26}$$

Same procedure can be applied to the stress as follows.

$$\sigma_c = C_c : (\varepsilon_c - \alpha_c \delta T) \tag{2.27}$$

Using 2.24

$$\sigma = \langle \sigma_c \rangle = \langle C_c : \varepsilon_c \rangle - \langle C_c : \alpha_c \rangle \delta T \tag{2.28}$$

Equations 2.26 and 2.28 are completely general under the assumption that uniform distribution of the stress and strain inside the grain. To solve the problems, different models are developed that is going to be explained as follows.

2.3.1. Isostrain and Isostress models

In here interaction part of isostrain (Taylor) and isostress (Sach) models is going to be considered. Since Taylor have different postulates on the deformation of polycrystalline, it would be better to state which part is going to be considered. Both of the models are rough estimates of the poly-crystal deformations, and most of the time gives upper and lower boundaries for stress-strain responses. Upper-lower boundaries are important because they give the interval where the overall stiffness of the aggregate must be.

2.3.1.1. Isostrain model. Taylor's isostrain model which is also known as Voigt's interaction model is one of the representations of the grain interactions. Model asserts that strain state of all grains are equal even their orientations differ. In other words, applied strain on the boundary is same for every crystallite. This postulate ensures the strain compatibility and this much enforcement to the strain brings sacrifice from the equilibrium condition.

$$\varepsilon_c = \varepsilon \tag{2.29}$$

Equation 2.28 can be written using 2.29 as in 2.30 since strain is equal in everywhere.

$$\langle \sigma_c \rangle = \langle C_c \rangle : \varepsilon - \langle C_c : \alpha_c \rangle \delta T$$

$$C : \varepsilon - C : \alpha \delta T = \langle C_c \rangle : \varepsilon - \langle C_c : \alpha_c \rangle \delta T \tag{2.30}$$

From Equation 2.30 overall stiffness and thermal coefficient matrix can be given as:

$$C^V = \langle C_c \rangle$$

and (2.31)

$$\alpha^V = {C^V}^{-1} : \langle C_c : \alpha_c \rangle$$

In Figure 2.5a two springs are placed parallel to each other. Both of them subjected to the same strain states. Analogy can be established for the fiber like grains in the coming Sections.

2.3.1.2. Isostress model. Isostress model of Sach which is also known as Reuss interaction model is one of the representations of the grain interactions. Model asserts that stress state of all grains are equal even their orientations differ. In other words, applied stress on the boundary is same for every crystallite. This postulate ensures the equilibrium condition and this much stress continuity enforcement brings sacrifice from the strain compatibility.

$$\sigma_c = \sigma \tag{2.32}$$

Equation 2.26 can be written as :

$$\langle \varepsilon_c \rangle = \langle C_c^{-1} : \sigma_c \rangle + \langle \alpha_c \rangle \delta T$$

$$C^{-1} : \sigma + \alpha \delta T = \langle C_c^{-1} \rangle : \sigma + \langle \alpha_c \rangle \delta T \tag{2.33}$$

Equating the same terms will end up with

$$C^R = \langle C_c^{-1} \rangle^{-1}$$

and (2.34)

$$\alpha^R = \langle \alpha_c \rangle$$

In Figure 2.5b two springs are placed serially. Both of them subjected to the same stress states. Analogy can be established for the penny-shaped grains in the coming Sections.

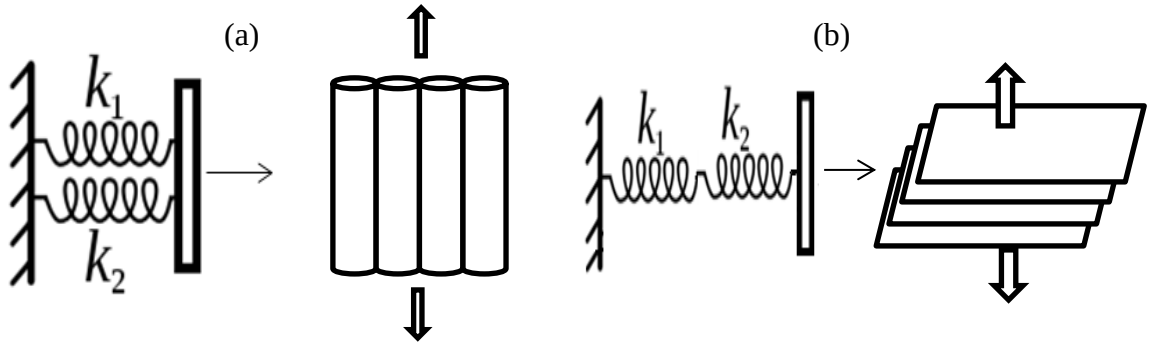

Figure 2.5. Spring analogy for (a) Isostress behavior of fibers (b) Isostrain behavior of layered morphology.

Both of these extreme cases isostrain (Taylor/Voigt) and isostress (Sach/Reuss) assumptions can be equal only when the crystal structures are isotropic. By isotropy, it is meant that any orientation scheme ends up with the same elastic constants. As a result taking the average of the inverse of crystal stiffnesses becomes same as the inverse of the average of the crystal stiffnesses.

It would be helpful to declare the Hill approach in here. Since Hill's assumption is used as a first assumption to sparkle the numeric model. Hill states that the upper-lower bands in metals are not great apart thus arithmetic averages of the Taylor/Voigt and Sach/Reuss can be used to estimate the overall stiffness [29].

$$C^H = \frac{1}{2}[\langle C_c^{-1}\rangle^{-1} + \langle C_c\rangle] \tag{2.35}$$

However, Hill's estimate fulfills neither the isostrain nor isostress; it is a nice initiator for the numerical models.

2.3.2. Self –Consistent Model

Self-Consistent model is another polycrystal model that does not rely on the uniform stress or strain throughout the polycrystal but relies on the Eshelby's exact solution which is uniform strain induced inside an elliptic inclusion due to the macroscopic loads within an infinite, homogenous medium. Since the method is based on the Eshelby's work, it would be worthwhile to examine the Eshelby's problem.

2.3.2.1. Eshelby Inclusion Model. In Eshelby's problem, which is a classical solution of linear elasticity, an ellipsoidal region (called an "inclusion") in an infinitely large domain is imposed to an eigenstrain and the stresses in the inclusion are solved. The stresses are proven to be uniform in the inclusion and expressed in terms of the imposed eigenstrains [9].

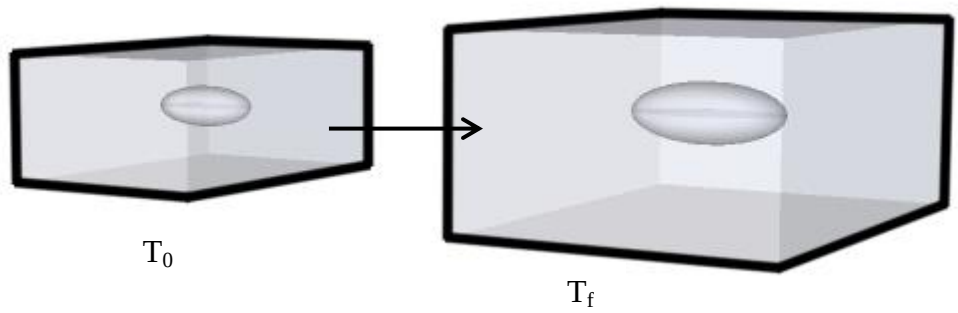

Figure 2.6. Imposing eigenstrain to an ellipsoidal inclusion by means of a thermal load.

Before starting the use of eigenstrain concept, it is valuable to state the Green function [30,31] that is used by Eshelby for the solution of the inclusion problem. One of

the powerful tools for solving the boundary problems in elasticity is the Green function. It is a general solution for even inhomogeneous boundary conditions i.e. unit point loads. There are various solutions for the Navier equation (Equation 2.37) but a generic solution to all kind of the boundary problems is coming with the Green function usage. Due to the linearity of the problem, that is no boundary condition and the material behavior dependency, which allows using the superposition principle by convoluting the specific solutions for each unit point force.

$$\sigma_{ij,j} + f_i = 0 \tag{2.36}$$

Equation 2.36 is the equilibrium equation where σ_{ij} is the Cauchy's stress tensor and f is the body force and throughout this work Einstain summation convention is used to state equations. A specific version of the above equation for isotropic linear elastic medium is the Navier equations.

$$(\lambda + \mu)\nabla(\nabla \cdot \boldsymbol{u}) + \mu\nabla^2\boldsymbol{u} + \boldsymbol{f} = \boldsymbol{0} \tag{2.37}$$

where λ and μ are the elastic constants for the isotropic medium. $\boldsymbol{u}$ is the displacement field. A specific body force vector at a point can be expressed as $f(\boldsymbol{r}) = f_0\delta(\boldsymbol{r})$ and the displacement can be expressed in terms of Green function for this unit load is denoted as $G_{ij}(\boldsymbol{r})$ where i is the ith component of the displacement and the j is the jth direction of the applied unit force. As can be seen, Green function differs from the original displacement field $\boldsymbol{u}$ by containing the load information. Replacing $\boldsymbol{u}$ with the G_{ij} and body force term with the unit body force ends up with :

$$(\lambda + \mu)\frac{\partial^2}{\partial x_i \partial x_k}G_{kj} + \mu\frac{\partial}{\partial x_m}\frac{\partial}{\partial x_m}G_{ij} = -\delta_{ij}\delta(r) \tag{2.38}$$

By applying a series of Fourier transformation and back-transformations Green function is solved for the unit constant point force and for isotropic homogenous medium as

$$G_{ij}(\boldsymbol{r}) = \frac{1}{8\pi\mu(\lambda+\mu)}\left[(\lambda+3\mu)\frac{\delta_{ij}}{r} + (\lambda+\mu)\frac{x_i x_j}{r^3}\right] \tag{2.39}$$

To see further detail one can see the [32]. What we have found up to this point is that a displacement field solution for a one specific load, linear nature of the problem enables us to convolve all of the loads by using the integral formula as:

$$u_i(x) = \int_{\Omega} G_{ij}(x - x')f_j(x')d^3(x') \tag{2.40}$$

where x' is the point where the body force acts. Inserting Equation 2.39 inside 2.40 one can find the overall displacement field for an arbitrary load. Since above equations are for only isotropic and infinite mediums, it needs to be extended to the anisotropic mediums. The notion of eigenstrain is a novel approach to find an equivalent homogenous medium for the inhomogeneity introduced medium.

The "eigenstrain" is an inelastic strain that is a term reserved for any type of strain that does not give rise to stress, such as thermal strains, phase transformations, plastic strains and misfits. In the literature other names are used like stress-free strains, transformation strains. One of the applications for the eigenstrain is the Eshelby's inclusion theorem where the overall theory is based on the eigenstrain imposition. In the Eshelby's inclusion theorem [9] the term transformation strains is used instead of eigenstrain. Eigenstrain permits us to solve elasticity problems where the heterogeneities such as dislocations are considered, by replacing heterogeneities with the equivalent body-forces.

To picture, consider an unbounded, linear elastic solid is subjected to a thermal load on a specific point on the material as in the Figure 2.6. The elliptic part of the solid is called inclusion and the medium around the inclusion is matrix. In the first stage of the problem only homogenous matrix is considered so the stiffness of inclusion and matrix are same. The question is what the stress distribution on the surface of the inclusion will be,

given the matrix will not freely allow the extra eigenstrain. Bearing in mind that stress is stemming from the elastic deformation one can equate the total strain to

$$\varepsilon_{ij} = \varepsilon_{ij}^{e} + \varepsilon_{ij}^{*} \tag{2.41}$$

where $\varepsilon_{ij}^{e}$is the elastic strain and the ε_{ij}^{*} is the transformation strain of the inclusion. A sketch to physically portray the theory is shown in Figure 2.7. Famous cutting, straining and welding procedure is exemplified:

(i) Cut out the ellipsoidal region Ω from the infinite medium V releasing all the constraints on it.

Matrix	Inclusion
$\varepsilon_{ij} = 0$	$\varepsilon_{ij} = 0$
$\sigma_{ij} = 0$	$\sigma_{ij} = 0$

(ii) Then the region is expanded due to eigenstrain, label ε^{*} as in the figure. In its new size, the ellipsoid is stress free since eigenstrains are any strain but those that impose stress.

Matrix	Inclusion
$\varepsilon_{ij} = 0$	$\varepsilon_{ij} = \varepsilon_{ij}^{*}$
$\sigma_{ij} = 0$	$\sigma_{ij} = 0$

(iii) To fit Ω back into V, it is applied (imaginary) tractions **T** on its surface to its

Matrix	Inclusion
$\varepsilon_{ij} = 0$	$\varepsilon_{ij} = \varepsilon_{ij}^{el} + \varepsilon_{ij}^{*} = 0$
$\sigma_{ij} = 0$	$\sigma_{ij} = C_{ijkl}\varepsilon_{ij}^{el} = -C_{ijkl}\varepsilon_{ij}^{*} = -\sigma_{ij}^{*}$

original size. So the traction force on Ω is $T_i = \sigma_{ij}n_j = -\sigma_{ij}^{*}n_j = -C_{ijkl}\varepsilon_{kl}^{*}n_j$ can be represent with the eigenstrain.

(iv) After reinserting, these imaginary forces are taken away, which means the inclusion will try to expand back to ε^{*}. However, it will be now resisted by the matrix and will only be able to expand to ε^{I}. But the traction on the inclusions surface is –T because from step 3 to 4 removal of the traction that keeps the inclusion in its original shape applies a cancelling opposite body force.

Matrix	Inclusion
$\varepsilon_{ij} = \varepsilon_{ij}^{I}$	$\varepsilon_{ij} = \varepsilon_{ij}^{I}$
$\sigma_{ij} = \sigma_{ij}^{I}$	$\sigma_{ij} = \sigma_{ij}^{c} - \sigma_{ij}^{*} = C_{ijkl}(\varepsilon_{ij}^{I} - \varepsilon_{ij}^{*})$

Body-force equivalents on the surface of the inclusion can be represented with:

$$f_j = C_{ijkl}\varepsilon_{kl}^{*}\delta(x_i)n_i \tag{2.42}$$

where n_i shows the normal of the surface and f_j is the body force which is zero everywhere except on the surface.

To find the final form of the inclusion and the overall displacement field new body forces are accounted around the Ω. These body forces can be represented by using the Green function explained above in Equation 2.40 yields:

$$u_i(x) = -\int_{\Omega} G_{ij}(x - x')C_{mjkl}\varepsilon^*_{kl}\delta(x_m)n_m d^3(x') \tag{2.43}$$

And if the eigenstrain is uniform and isotropic medium, Equation 2.43 can be written as:

$$u_i(x) = -C_{ijkl}\varepsilon^*_{jk}n_k \int_{\Omega} G_{ij}(x - x')d^3(x') \tag{2.44}$$

Consequently, the displacement field can be represented in terms of the eigenstrain of the inclusion. So the total strain inside the inclusion can be cast as a linear relation in terms of the eigenstrain or transformation strain using a 4th order Eshelby tensor S which is dependent only to the stiffness of the aggregate and the inclusion geometry, and eigenstrain is used to give the body-force effects on the inclusion. Thus relates the final contracted inclusion shape to the original shape mismatch between the matrix and the inclusion.

$$\varepsilon^c_{ij} = S\varepsilon^*_{ij} \tag{2.45}$$

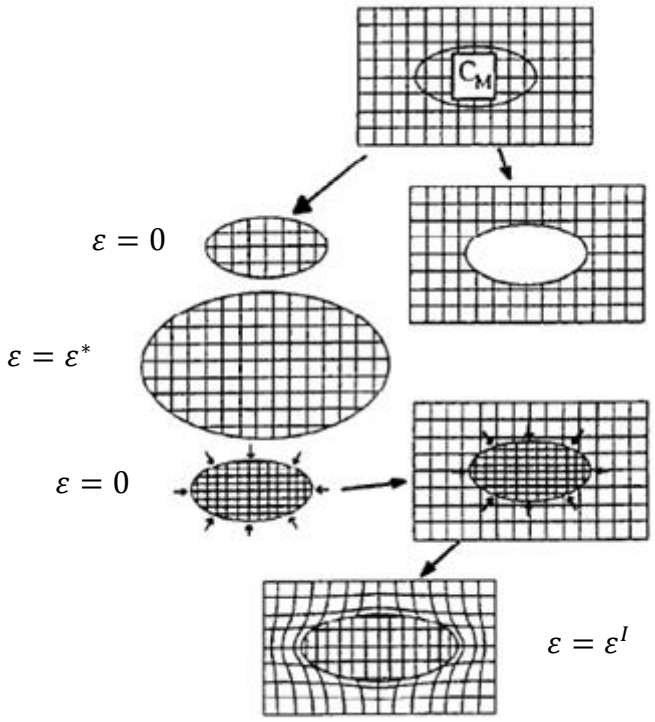

Figure 2.7 Cutting and welding exercises for an inclusion with imposed eigenstrain in an effective medium of the same stiffness tensor. (reproduced from [33])

Up to this point, homogenous medium with a stiffness of $\mathbf{C_M}$ and inclusion with the same elastic property is loaded with an arbitrary inelastic strain. As a result a mismatch between the matrix and inclusion is occurred. This leads to a scramble for sharing the amount of the strain. Final form of the strain sharing can be expressed with an Eshelby tensor which relates the total strain to the inelastic strain (eigenstrain). However, in reality most of the metals are anisotropic, which means having different stiffness of the inclusion ($\mathbf{C_I}$) than the stiffness of the medium ($\mathbf{C_M}$). Theory is further developed with the idea of finding an equivalent homogenous medium by using the eigenstrains (transformation strain).

2.3.2.2. Inhomogeneity Problem: Grain in HEM. The grain in HEM is actually not similar to the Eshelby problem. Here, the elastic stiffnesses of the grain ($\mathbf{C_I}$) and HEM ($\mathbf{C_M}$) are different unlike the Eshelby problem. When a subdomain Ω has elastic moduli different from those of the matrix, it is called an inhomogeneity.

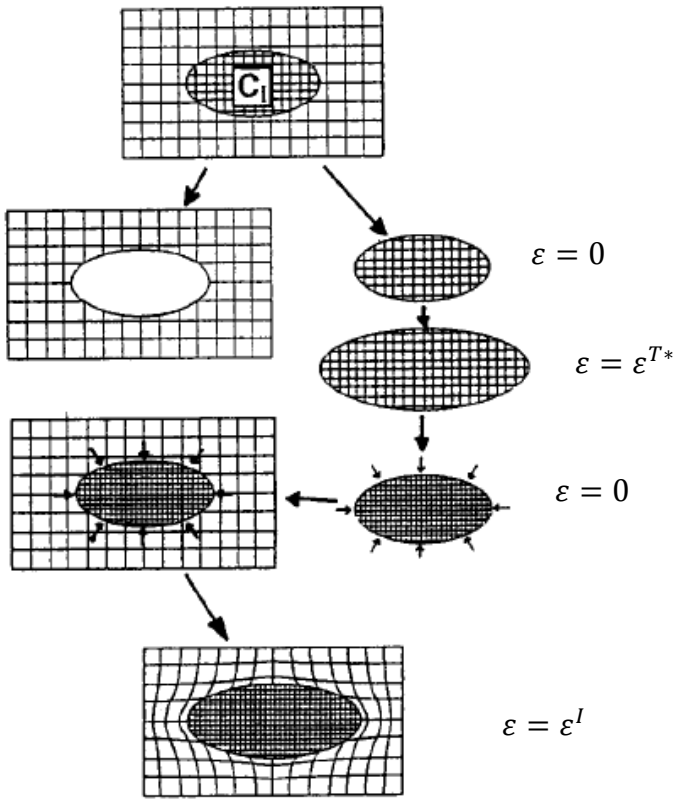

Figure 2.8. Cutting and welding exercises for finding an equivelant homogenous medium for the inhomogenous inclusion problem. (reproduced from [33])

Using Eshelby inclusion model is not straightforward for the inhomogeneity problems. However, this can be exceeded (described in Fig. 3) by some modifications mostly trying to find an equivalent Eshelby model given the fact that, in both problems the stresses/strains are constant inside the considered ellipsoidal regions. This means the inhomogeneity problem that is described with (C_I, C_M, ε^{T*}) can be converted to an equivalent Eshelby inclusion problem with (C_M, C_M, ε^*). Equivalent means simply that the inclusion in the equivalent problem has the same uniform stress as the inhomogeneity in the physical case feels. The task is finding the appropriateε^*.

Since the stress field around the inclusion in homogenous medium is :

$$\sigma_M = C_M(\varepsilon^I - \varepsilon^*) \tag{2.46}$$

and the stress field around the inhomogeneity is

$$\sigma_I = C_I(\varepsilon^I - \varepsilon^{T*}) \tag{2.47}$$

Using Equation 2.45 and equating 2.46 and 2.47

$$C_I(S\varepsilon^* - \varepsilon^{T*}) = C_M(S - I)\varepsilon^* \tag{2.48}$$

where I is the identity tensor.

The equivalent homogenous transformation strain can be expressed in terms of the inhomogeneous inclusion. Stress inside the inclusion can be calculated by proper arrangement of Equation 2.48 yields

$$\sigma_I = C_M(S - I)[(C_I - C_M)S + C_M]^{-1}C_I\varepsilon^{T*} \tag{2.49}$$

This inhomogeneity problem can be extended to the applied load. Since this time elastic strains are imposed by the loading, further calculations are required. But main logic is that find an equivalent medium that gives the same stress-strain state by finding this medium apply the same Eshelby procedure above find the displacement field. Although solution procedure is for an elastic problem it can be extended to the plastic regime by introducing the instantaneous stiffness L and the rate of the stress and strain.

Returning back to the Self-Consistent modeling, work of Eshelby is introduced to the model as pointed out in section Self Consistent Models 1.2.1.2. Each inclusion (C_I) is behaved as an inhomogeneity and their averages represent the overall response of the aggregate. Stress and strain rates are related with an instantaneous stiffness matrix for the medium and the inclusion, respectively as:

$$\dot{\sigma} = L\dot{\varepsilon}\ ,\ \dot{\sigma}_c = L_c\dot{\varepsilon}_c \tag{2.50}$$

where $\dot{\varepsilon}$ is the macroscopic strain rate and $\dot{\varepsilon}^c$ is the strain rate of the inclusion. Discrepancies in between the medium and the inclusion are related by a constrained tensor (effective stiffness) L^* :

$$(\dot{\sigma} - \dot{\sigma}_c) = -L^*(\varepsilon - \varepsilon_c) \tag{2.51}$$

also

$$L^* = L(S^{-1} - I) \tag{2.52}$$

where L^* is coming from the theory that is total discrepancies has to be zero. Plugging 2.50 into 2.51

$$\dot{\varepsilon}_c = (L_c + L^*)^{-1}(L + L^*)\dot{\varepsilon} \tag{2.53}$$

Equation 2.53 gives the relation in between the macroscopic strain rate and the crystal strain rate. This relation can be cast into a 4th order localization matrixA_c.

$$A_c = (L_c + L^*)^{-1}(L + L^*) \tag{2.54}$$

$$\dot{\varepsilon}_c = A_c\dot{\varepsilon}$$

Using 2.54, stress rate of the crystal becomes

$$\dot{\sigma}_c = L_c A_c \dot{\varepsilon} \tag{2.55}$$

The final step in the formulation is taking the fractional averages of the stress and strain rates of the crystals to obtain the macroscopic quantities.

$$\begin{aligned} \dot{\sigma} = \langle\dot{\sigma}_c\rangle \Rightarrow L = \langle L_c A_c\rangle \\ \dot{\varepsilon} = \langle\dot{\varepsilon}_c\rangle \Rightarrow L^{-1} = \langle {L_c}^{-1} {A_c}^{-1}\rangle \end{aligned} \tag{2.56}$$

The ultimate goal of the SCM is to find the L (overall stiffness) but L^* and S depend on the overall stiffness. Therefore an iteration procedure is required till a convergence is reached. An independent estimate is done for the thermal expansion coefficient as:

$$\alpha = L^{-1}\langle (L^* + L_c)^{-1}\rangle^{-1}\langle (L_c + L^*)^{-1} L_c \alpha_c \rangle \tag{2.57}$$

where α is the overall thermal coefficient tensor and α_c is the crystal thermal coefficient tensor.

3. NUMERICAL

3.1. Generic Procedure of Point Models

In point models, the constitutive behavior of the material is modeled at the grain level and the overall behavior of the aggregate is averaged from the calculated behavior of individual grains. Hence, there are two primary modeling components: (i) constitutive behavior of the crystals, and (ii) interaction with the aggregate. The former is related to the crystal (member) elastic-plastic properties and the latter governs the consistent averaging of the members (cluster). All of the point models have to include both of these. In this section, the more generic names ‘cluster’ and ‘member’ are adapted for aggregate and grain, respectively. (This is done for a future extension of the APMF to hierarchical interaction where each member is not necessarily a grain.)

Point models are primarily characterized with the interaction component (isostress, isostrain or Eshelby are interaction types). However, of course, the constitutive law (e.g., hardening law) carries the fundamental physics of deformation (slip/twinning modes and their hardengin laws.) Through the consideration of alternative rules, for instance, isotropic or kinematic hardening for constitutive model; isostress or isostrain assumption for interaction model, one can scan a wide range of problems.

Point model calculations are based on a three-layer nested loop that is defined by the time stepping. First loop is the step loop; steps are description of distinct thermo-mechanical processes with different boundary conditions. The second loop is the increment loop; each step is subdivided to increments allowing to process the boundary conditions gradually for the solution of this nonlinear problem. The third loop, which is the core of the code, is the iteration loop that calculates the instantaneous stiffness matrix of the members and the cluster. The iteration loop is ended at the point they are “self-consistent”. The flowchart in

Figure 3.1 represents the algorithm used in the point models. The dashed part shows the second loop where the load increments are applied.

At the beginning of the process, initialization of the variables is handled which includes the processing of inputs and preliminary tensorial calculations (e.g., the elastic stiffness of members are calculated). The first operation in the loop (BC) requires a cluster (member-averaged) stiffness. Hence, initialization procedure includes also coordinate transformations due to the requirement that operations on tensors should be conducted on their components in the same coordinate system (CS). This means member stiffnesses, that are input in the crystal CS are transformed on the sample CS using the orientation data. Following that their consistent averaging is performed to find cluster stiffness.

Time loop inside a deformation step:

- *BC*: The displacement/force boundary conditions are then considered along with averaged moduli to calculate the unknown stress/strain components of the cluster.
- *Interaction-Localization*:Then, the strain/stress in each member is determined with the proper 'localization' component of the interaction model. Over all members, in the constitutive part, individual stiffness and stress-strain states are determined based on the input elastic-plastic behavior.
- *Constitutive part*: is structured on the plastic flow of stress. Indication of the plasticity is the 3rd condition in Equation 2.14. Amount of the shear resolved on the slip plane in each member determines the active planes. After then the naming of the active planes for each grain orientation family, shear strain rates on them is determined by the projection of the total strains using f in Equation 2.20. f is dependent on the hardening law used in the model.
- *Interaction-Averaging*: The basis of the interaction part is as stated in the above sections: isostress, isostrain or Eshelby equivalent inclusion formalism. Average of the stiffness values (Equation 2.31, 2.34, 2.56) are taken depending on the which formalism is used.
- *Convergence* :Once, this loop is complete, If the convergence of the cluster stiffness is achieved then the next load increment can be applied to the cluster. If the

convergence is not achieved then the new stiffness and localization (A_c) matrices are iterated until a convergence is reached.

- *Database* : Response of the members and the cluster has to be recorded in order to use inside a post-process. Hence, a storing capability has to be inside the models.

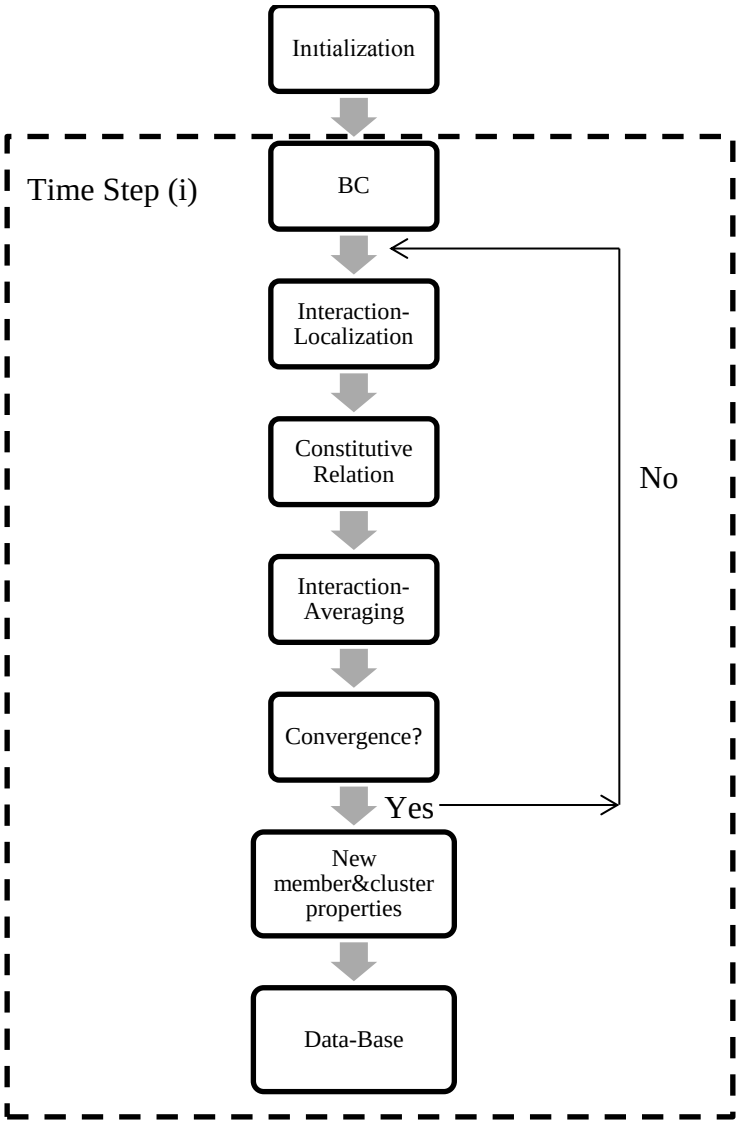

Figure 3.1. Flowchart of the code; the dashed box contains the processes inside a load increment.

3.2. Languages

In this work two programming languages are used: FORTRAN and Python. FORTRAN is an essential programming language prepared for to numeric computations as the name implies (Formula Translating System). It is one of the fastest languages in this area. However, it is hard to read and not user-friendly which becomes crucial while writing a huge code. On the other hand, Python is a high-level, interpreted, interactive and object-oriented-scripting language. Firstly it is an object-oriented language which enables to reflect the physical sense of the theory to the coding environment. Secondly it provides flexibility to work with other programming languages. Since EPSC is constructed from the many nested loops, reflection of the physical sense or the flexibility is not enough but also speed is required. To overcome this problem, we used the F2py module of the python of which establishes an easy connection in between the Python and FORTRAN. Combination of the best sides of both languages intersects on the usage of F2py. Loop operations are performed by FORTRAN via using F2py; physical sense is conserved with the Python in addition to flexible changes in the models.

3.3. Adaptable Point Model Framework

EPSC3 is a FORTRAN-77 computer code which is written by C. N. Tome and P. Turner in 2002. It is an implementation of the self-consistent model that can calculate the thermo-mechanical response of a single-phase material with elastic-plastic constitutive behavior. It found wide use in the scientific community particularly in connection to evaluating mechanical tests with in situ neutron diffraction data [20,34-36]. EPSC3 works in the elastic-plastic region where the deformation is small. EPSC3 is a tested code that is restricted to single-phase materials. Further, being a legacy code in FORTRAN, the subroutines are fixed in the code; and hence, it is not easy to interchange a function (or a model component) with its alternative. Another main problem is the post-processing part of the EPSC3; the structure and parameter content of the EPSC3 output are strictly defined before the run. Hence, it is not possible to tailor which variables will be output and their detail level.

To transcend the restrictions of straightforward EPSC3, a new framework is developed here, called APMF (Adaptable Point Model Framework) using a combination of Python and FORTRAN languages. Python is an object-oriented language that allows implementation of (using *class* structures) point model hierarchy, model interchangeability, and data base interaction. At the bottom of the hierarchy, a *member* class resides, which constructs the micro-scale of the meso-scale model. The *member* class contains the properties of each member, e.g. elastic stiffness of the members. On top of the member class, a *cluster* class is founded which establishes the meso-scale of the model, e.g., boundary conditions are imposed on the cluster. Object-oriented programming has the fundamental future of inheritance. For example, once a base *cluster* class is formed; *cluster* classes for different models can be inherited.

Depending on the interaction or the constitutive law, inherited classes serve to case-specific needs; e.g., while Eshelby interaction uses ellipsoids, isostrain interaction does not use inclusion theory hence, there is no need to for ellipsoidal information of the members. After these classes are generated, each *member* and *cluster* instance contains the necessary physical properties as parameters. Post-processing contains gathering data from the very detailed output of large number of members in this case. Another Python class written for this purpose is the *database* class which determines the recorded output parameters and their recording frequency (each increment, only once, etc.). Database usage is extremely important in the post-process part because of dealing with vast amount of data and the PyTables package is used ([37]). The data entries of the *member* and the *cluster* parameters in the database are coded in an entirely configurable fashion. For example, localization matrix of each member can be specified to be input to the data base, or not. PyTable enables us to deal with hierarchical datasets efficiently and easily cope with extremely large amounts of data.

In addition to the three main loop structure, there are also sub operations with large for loops and if-else statements that take considerable computational time. At this point, APMF uses wrapping of FORTRAN routines with F2py since FORTRAN is fast with mathematical operations and loops. Subroutines inside the core loop are wrapped by

manipulating the inputs and outputs of the FORTRAN subroutines according to the class concept in Python.

The primary capabilities of APMF are:

- The code admits multiple phases with different elastic stiffness and slip systems.
- The existing self-consistent schemes that were described in Section 1.2.1 are implemented. Also, the code is flexible enough to put together any hierarchy.
- Although immediate results are targeting EPSC and isostress/strain models, the modularity should allow for inserting VPSC as the constitutive model easily.
- The code is fast enough. Python as an interpreted language is not built for speed as compiled languages and particularly bad with loops. Time-consuming basic FORTRAN functionalities (such as taking the stiffness average of all grains, rotations, etc.) are wrapped in PYTHON for speed.
- Different thermo-mechanical experiments can be conducted via giving different loading conditions in the process loop.
- Post-processing parameters can be hand-picked based on each application.

4. RESULTS & DISCUSSION

This section comprises the evaluation of structural capabilities of the developed APMF software through several *test cases*. To create a basis, first, the morphological capability of EPSC3 is evaluated for a single-phase material in comparison with the results of limiting-case point models of isostrain and isostress. Then, multi-phase cases are considered which present the value of the current framework.

The total of 10 test cases is tabulated in Table 4.1 with the case numbers shown in the first column. The texture of a case (random or fiber in our context) is indicated in the "Texture" column. Tested grain interaction types are isostrain, isostress and Eshelby. Eshelby ellipsoidal inclusion (EEI) radii and orientations will be detailed in the related sections. Cases 1 and 2 are the extreme (isostress and isostrain) cases that give upper and lower stiffness bounds. Limiting bounds are presented for the reason that, it is very helpful while explaining the behaviors of the ellipsoidal morphologies (Cases 3-10). Third case uses spherical inclusions as in Figure 1.4a to model the equiaxed grains. Fourth case, fiber shaped grains (Figure 1.4b) of aggregate is mimicked by using a needle-like inclusions (Figure 1.5b). Fifth case is showing the thin layer of single phase (Figure 1.4c) material representation by using disc-shaped inclusions (Figure 1.5c). Sixth case is transversely isotropic case with 111-fiber texture (Figure 1.4b with fibers oriented along 111 directions). Seventh to tenth cases are the models of multi-phase materials (Figure 1.4 d-h). These test cases are evaluated in the following sub-sections.

Table 4.1. 10 test cases evaluated with APMF. In column 6 and 7, EEI is the abbreviation for Eshelby Ellipsoidal Inclusion.

#	Material	# Grain	Texture	Interaction	EEI radii	EEI Orientations
1	Cu	8000	Random	Isostrain	NA	NA
2	Cu	8000	Random	IsoStress	NA	NA
3	Cu	8000	Random	Eshelby	1,1,1	0,0,0
4	Cu	8000	Random	Eshelby	15,1,1	0,0,0
5	Cu	8000	Random	Eshelby	1,15,15	0,0,0
6	Cu	8000	Fiber	Eshelby	1,1,1	0,0,0
7	Cu+Nb	5000+5000	Random+Random	Eshelby	(1,1,1)+(1,1,1)	(0,0,0)+(0,0,0)
8	Cu+Nb	5000+2500	Random+Fiber	Eshelby	(1,1,1)+(15,1,1)	(0,0,0)+(0,0,0)
9	Cu+Nb+Nb	5000+2500+2500	Random+Fiber+Fiber	Eshelby	(1,1,1)+(15,1,1) +(15,1,1)	(0,0,0)+(90,-45,90) +(90,45,90)
10	Cu+Nb	5000+5000	Fiber+Fiber	Eshelby	(15,15,1)+(15,15,1)	(0,0,0)+(0,0,0)

For uniformity and easy interpretation of the results the materials studied are limited to Copper for single-phase cases and Copper/Niobium for the two phase cases. Both these materials exhibit high levels of elastic anisotropy. Using Equation 2.1 Cu and Nb have an anisotropy ratio of 0.49 and 3.21, respectively. As pointed out in Section 2.1, deflection from the value of 1.0 of the anisotropy ratio reflects the behaviors of different orientations. The used hardening parameters in the models are coming from the Hall-Petch relation.

$$\sigma_y = \sigma_0 + kd^{-1/2} \tag{4.1}$$

where σ_y is yield stress, σ_0 is the frictional stress required to move the dislocations, k is the slope and d is the diameter of the grain size. Values in Table 4.2 are used to obtain τ_0 with a 2 μm diameter grains for both of the Cu and Nb. Remaining parameters are

attuned such that a sensible yielding scheme is created as in Table 4.3. E_{rnd} in Table 4.3 corresponds to the Young modulus of the Cu and Nb clusters where the inclusion shapes are spherical.

Table 4.2. Parameters for Hall-Petch relation.

	σ_0(Mpa)	k(MNm$^{3/2}$)
Cu	25.5	0.11
Nb	68.64	0.04

Table 4.3. Elastic stiffness and hardening parameters for Cu and Nb.

	Elastic Stiffness (GPa)				Hardening Parameters			
Material	C_{11}	C_{12}	C_{44}	E_{rnd}	τ_0(MPa)	τ_1(MPa)	θ_0	θ_1
Cu	240.2	125.6	28.2	129.7	50	100	1.0	0.001
Nb	168.4	121.4	75.4	105.0	70	60	1.0	0.001

Textures are generated for both of the isotropic and transversely isotropic textures. Generated-isotropic cases are fulfilling the requirements when the number of grains is larger than 3000. Hence, selection of 8000 grains is adequate to represent. Orientation distributions for transversely isotropic textures are obtained from the Aydiner *et al.* [11]. Preferred textures for Cu is 111 and for Nb 110 created with using a Weibull distribution function. In Figure 4.1, ψ is the angle indicating the deviation from the sample coordinate axis-1.

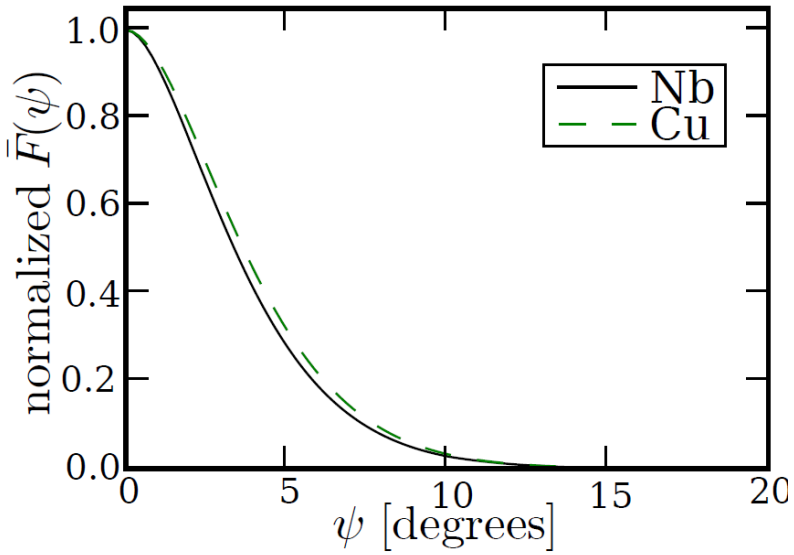

Figure 4.1. Orientation distribution function, $\bar{F}(\psi)$, for phases Cu and Nb. (reproduced from [11])

Boundary conditions for the models should be given in terms of six components stress and strain, such that the remaining six are available through the constitutive relation. If the input is among the strains then from constitutive law stress information is gathered, vice versa is valid also. Except the final case in Table 4.1 (Cu layers with fiber-texture on Nb layers with fiber textures), boundary conditions for the cases tabulated are:

$$\varepsilon_{11} = 1.4 \times 10^{-3} t \; ; \; \sigma_{22} = \sigma_{33} = \sigma_{23} = \sigma_{13} = \sigma_{12} = 0 \tag{4.2}$$

where t is the step time ranging from 0 to 1. The final value of strain, 0.14%, is chosen as a moderate strain that will bring the materials to the initial stages of plasticity.

4.1. Isostrain/isostress Limit Cases

As pointed out in the above section, isostrain/isostress interactions are the two limiting cases in terms of the effective stiffness (isostrain stiffest, isostress softest) that are defined for polycrystalline aggregates [21]. For the evaluation here, two random-texture Copper aggregates are considered under uniaxial load (cases 1 and 2 in Table 4.1).

(*S*,*hkl*) is the notation used for depicting strain/stress results of individual grain sets. Here, *S* is a direction in sample coordinate system (CS) and *hkl* is a crystallographic plane family. (*S, hkl*) denotes the grain set whose *hkl* plane normals are aligned with *S*. When (*S, hkl*) is associated with a scalar strain/stress result, the average normal strain/stress of this grain set along direction *S* is implied. The direction *S* will be usually picked to be a sample coordinate axis. To exemplify, (1,111) strain depicted in Figure 4.2a shows the 11 component of normal strain averaged from grains whose {111} planes are normal to sample CS axis-1. In this case, the sample is also loaded along axis-1. In general, for cubics, to show intergranular stress/strain variations, it is optimal to consider grains whose {111} and {100} planes are normal to loading directions, since these exhibit the extremes of stiffness under uniaxial testing (Equation 2.2).

With isostrain, (1,111) and (1,100) strains are ordained to be the same as shown in Figure 4.2a. Note (2,hkl) and (3,hkl) where 2 and 3 are directions normal to the loading axis will yield transverse direction strains that are negative due to Poisson effect. (3,hkl) curves, however, are not shown in the figures, since they are identical to (2,hkl) with symmetry. (Recall random texture is assumed here.)

For Cu, <111> direction is the elastically stiffest and <100> is the elastically softest direction while <110> is in between two extremes (Equation 2.2). When the same strain state is imposed on all of the crystals, the stiffest grains (1,111) bear higher stress than other orientations do. This is clarified in Figure 4.2b which presents (1,111), (1,110) and (1,100) stresses where the former takes more stress than the others per average stress increment. To quantify, we define apparent modulus $\bar{E}_{hkl}$ and load fraction $L_{f\,hkl}$ as follows:

$$\bar{E}_{hkl} = \frac{d\sigma_{avg}}{d\varepsilon_{1,hkl}} \tag{4.3}$$

$$L_{f\,hkl} = \frac{d\sigma_{1,hkl}}{d\sigma_{avg}} \tag{4.4}$$

$\bar{E}_{hkl}$ is apparent as the slope of the (1 , hkl) curves in average stress versus grain-set strain plots such as Figure 4.2a. Its value is an indication of how much strain is induced inside individual grain-sets. $L_{f_{hkl}}$, on the other hand, is visible in average stress versus grain-set stress plots such as Figure 4.2b . It characterizes how stress is partitioned among grain sets (1,hkl) of different stiffness. Here, we note $L_{f_{hkl}}$ is the inverse of the slope of the curves of Fig. 4-1b.Thus, the shallower the slope the higher the load that grain set incurs (e.g., (1,111) curve in Figure 4.2b).

For all the interaction cases covered here (including Eshelby type interactions that will be covered in following subsections), apparent modulus $\bar{E}_{hkl}$ and load fraction $L_{f_{hkl}}$ are tabulated in Table 4.4 and Table 4.5, respectively. Isostrain case is covered in the first row of these tables. In these tables, $\bar{E}_{111}/\bar{E}_{100}$and $L_{f_{111}}/L_{f_{100}}$ reflect the separation of the (1,111) and (1,100) grain sets (the supposed extremes) for highlighting the nature of the assumed interaction. For example for isostrain, naturally $\bar{E}_{111}/\bar{E}_{100}$ is set to 1. But forcing strain equality results in large separation for stress ($L_{f_{111}}/L_{f_{100}}$ =1.99).

Table 4.4. Apparent moduli table, $\bar{E}_{hkl}$, for single-phase 1 point models that is considered in this thesis.

	$\bar{E}_{111}$	$\bar{E}_{110}$	$\bar{E}_{100}$	$\bar{E}_{111}/\bar{E}_{100}$
Isostrain	145.05	145.05	145.05	1.00
Isostress	188.56	129.90	67.12	2.81
Esh111	158.46	139.08	101.76	1.56
Esh1511	131.61	130.47	128.57	1.02
Esh11515	163.04	144.21	97.68	1.67
EshTI1511	190.15	168.76	125.40	1.52

Table 4.5. Load fraction table $L_{f_{hkl}}$ for single-phase 1 point models that is considered in this thesis.

	$L_{f_{111}}$	$L_{f_{110}}$	$L_{f_{100}}$	$L_{f_{111}}/L_{f_{100}}$
Isostrain	1.25	1.09	0.63	1.99
Isostress	1.00	1.00	1.00	1.00
Esh111	1.16	1.06	0.76	1.52
Esh1511	1.42	1.10	0.56	2.53
Esh11515	1.01	1.00	0.99	1.02
EshTI111	1.00	0.92	0.67	1.47

The change in the slope of any (*S*,hkl) curve in Figure 4.2b is associated with the aggregate plasticity in a complex manner. The slope of an individual grain set might change although that grain set is not necessarily exhibiting plasticity yet. Recall load fraction is the inverse of the slope, so if a (1, hkl) grain set shoots up with respect to its initial elastic slope, the interpretation is that the grain set is taking a smaller share of the average stress increment and plastic activity initiated in it. The grain set that shoots up first is (1,111) which has the highest elastic load fraction (1.25); it makes sense that the grain set that takes the highest share of stress yields first. The effect of the initiation of plasticity in (1,111) orientations is to shed stress to other grain sets. Hence, (1,100) oriented crystals take higher share of the average load (the curve leaning right, getting a higher load fraction), in the process of (1,111) grains yielding. Thus, the (1,100) initial slope change is not really related to (1,100) yielding but other grains sets yielding and shedding load to these elastically-soft grains. Under this additional stress, eventually (1,100) also yield indicated by the second change of slope in the (1,100) curve, this time upwards.

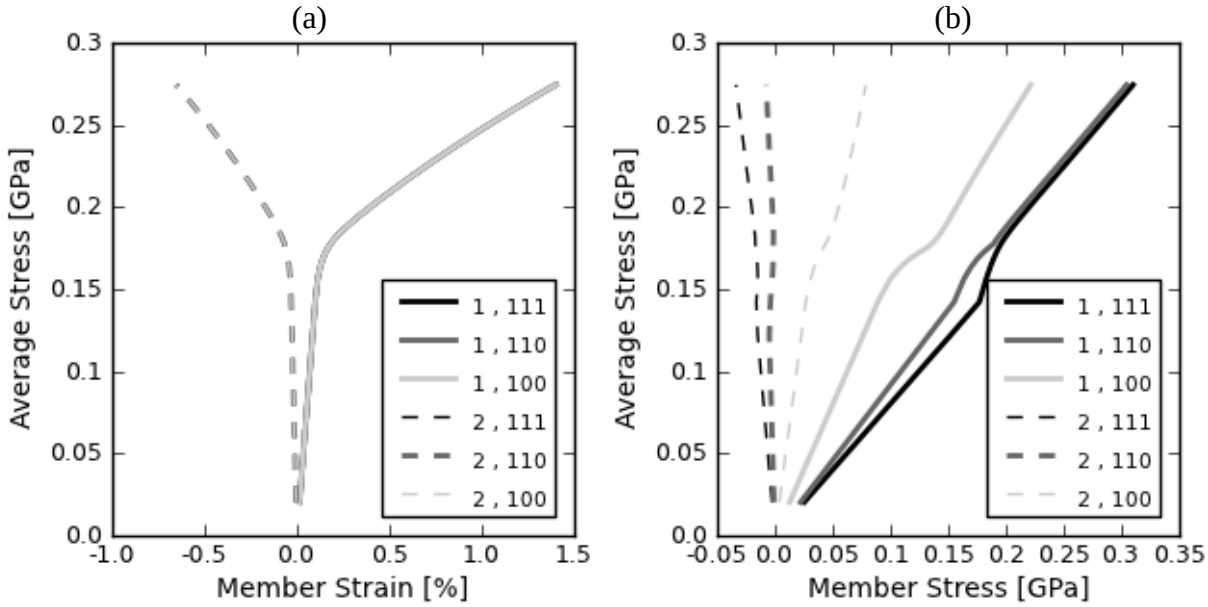

Figure 4.2. (a) Cluster average stress versus member strain , (b) average strain versus member stress on the specified grain sets (S,hkl). Isostrain interaction of single-phase Cu under uniaxial tension.

Corresponding plots for the complementary isostress interaction are in Figure 4.3. This time, grains inside the aggregate have the same stress state without depending on the orientation as shown in Figure 4.3b. (1,hkl) curves are coincident with load fraction of (1.00), (2,hkl)s are also coincident and zero. To obtain the same stress states in different orientations of grains, stiff grains carry less strain than soft grains along the loading axis 1. The according separation of strains of (1,111) and (1,100) can be seen in Figure 4.3a with ratio of slopes $\frac{\bar{E}_{111}}{\bar{E}_{100}}$ =2.81. Transverse direction also exhibits the same behavior since there is no competition in between grains of different sets just the load is equally distributed ($\frac{L_{f_{111}}}{L_{f_{100}}}$ =1.00).

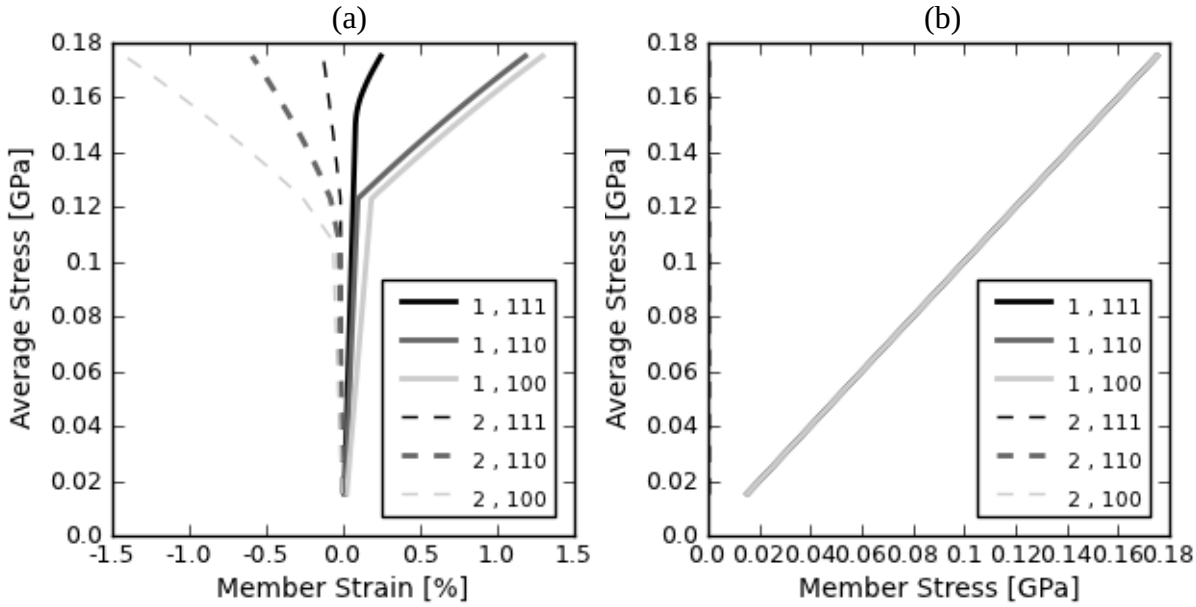

Figure 4.3. (a) Cluster average stress versus member strain on the specified grain sets, (b) average strain versus member stress on the specified grain sets. Isostress interaction of the (S,hkl) sets for single-phase Cu under uniaxial tension.

4.2. The Effect of Eshelby Ellipsoid Radii in Single-phase EPSC Model

In this section, capabilities of straightforward EPSC are stated, which is only capable of a single phase and can impose a single Eshelby ellipsoid to all cluster member (grains). Differing from the isostress/strain cases, in the self-consistent model (Section 2.3.2) grains compete to satisfy the equilibrium and compatibility conditions. As will be shown, one of the important factors in this competition is the dimensions of the Eshelby ellipsoids.

Grains have been statistically categorized as equiaxed, fiber (needle) shaped, and layer (disc) shaped as depicted in Figure 1.4a, b, c respectively. The corresponding Eshelby model can be formulated by adjusting the Eshelby ellipsoid ratios as shown in Figure 1.5a, b, c. Radii parameters used in Table 4.1 are the respective ratios of the ellipsoidal axes. 15 is used as a sufficiently large number, 15>> 1. In Table 4.1, 3rd, 4th, 5th rows employ random texture with the inclusions are in the shape of spherical (1,1,1), needle-like (15,1,1) and disc-shaped (1,15,15), respectively. Sixth case corresponds to a fiber texture where the individual grains are oriented such that (1,111) grain set is the

dominant set in the texture and it has an isotropy around the axis-1 (ND). By using limiting shapes with comparing the isostress/strain cases it is aimed to verify the morphology effect on the behavior of the polycrystals.

Straightforward EPSC has the capability of representing the basic morphologies for the single phase materials. One of them is the case-3 where (1,1,1) ellipsoid ratios are used with ellipsoid orientations of (0,0,0) in Eulerian angles. Corresponding results are figured in Figure 4.4. All of the (1,hkl) directions in Figure 4.4a show variation in strain (unlike isostrain case), but this variation is smaller than that of the isostress case. The opposite is also true, in Figure 4.4b (1,hkl) stresses on the members (i,hkl) show less separation than isostrain case. The (elastic) strain sharing level is decided by the elastic constants and the Eshelby interactions of the grain sets. From Table 4.4 and Table 4.5 we can see both of these effects. In Figure 4.4a slope of the (1,111) and (1,100) are, respectively 158.46, 139.08 and in Figure 4.4b slope of the (1,111) and (1,100) are, respectively 1.16, 1.06. The difference in the slope values is stemming from the stiffness properties of the directions. Although they are different, they are not separated as much as the isostrain/stress of the grain-sets in the Figure 4.3 and Figure 4.2. $L_{f_{111}}/L_{f_{100}}$ of isostrain case is 1.99 and $\bar{E}_{111}/\bar{E}_{100}$ of isostress case is 2.81 where Esh111(case-3) is 1.52, 1.56, resectively. In here, the effect of the grain-sets interaction can be seen which makes the curves closer with respect to the extreme cases. Stiffest obtains a lower member stress compared to what it would in isostrain interaction, meaning a higher slope than the isostrain case in the average stress vs. member stress curve and softest obtains higher member stress with lowering its slope as seen in Figure 4.4b.

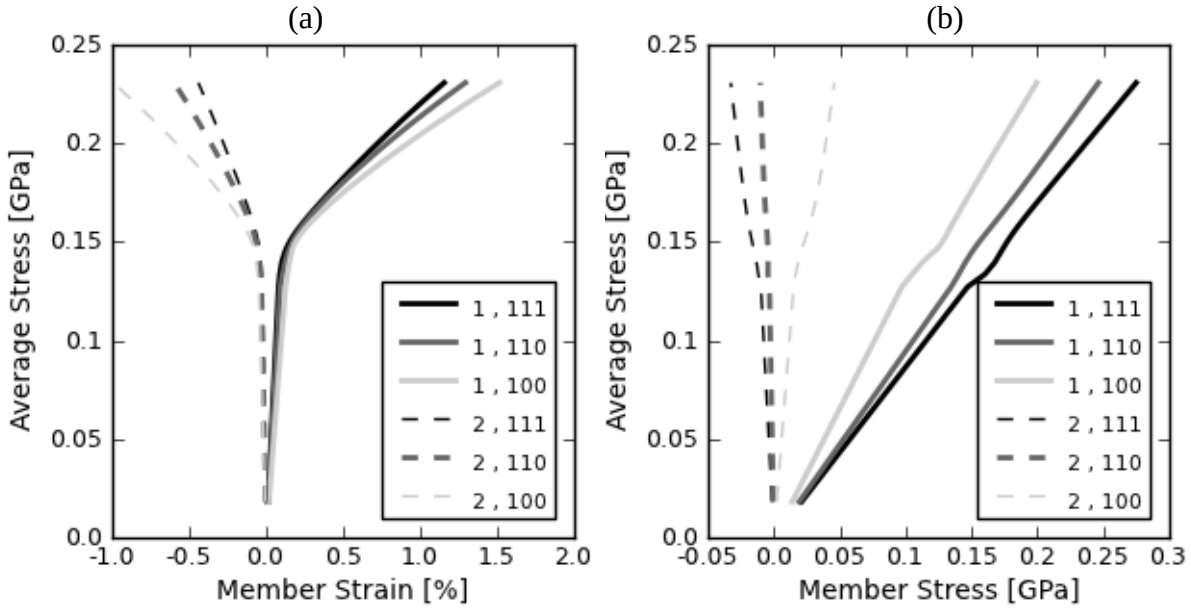

Figure 4.4. (a) Cluster average stress versus member strain, (b) average stress versus member stress on the specified (S,hkl)grain sets. Eshelby interaction with an inclusion shape of (1,1,1) for single-phase Cu under uniaxial tension.

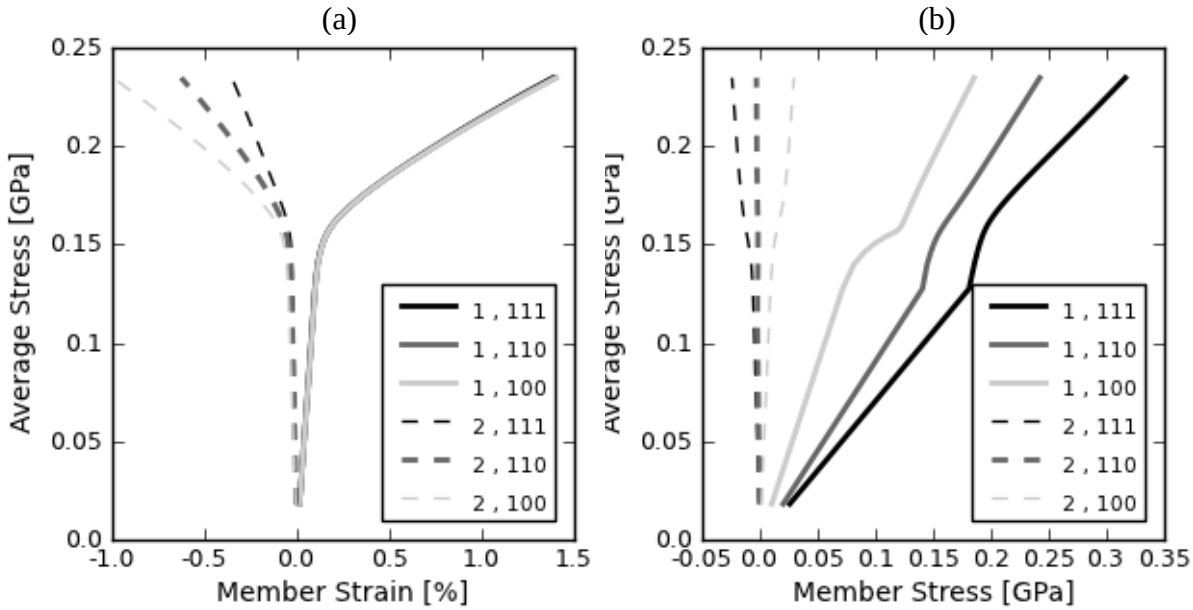

Figure 4.5. (a) Cluster average stress versus member strain , (b) average stress versus member stress on the specified (S,hkl)grain sets. Eshelby interaction with an inclusion shape of (15,1,1) for single-phase Cu under uniaxial tension.

For the fourth case, the inclusion has a shape of (15,1,1) , a needle-like inclusion. The tensile part of the Figure 4.5a shows that (1,111) and (1,100) directions are overlapped. This means that the grain-sets of the stiffest and softest directions deforms same but the stress on them is departed considerably as can be seen from the Figure 4.5b. This is the same as 2 springs with different constants that are placed parallel to each other and attached to a frame with load given from one end as in Figure 2.5a. The amount of the strain is same for the each spring. Although slopes of the curves (1,111) and (1,100) are close enough to reflect the parallel spring behavior (131.61 and 128.57, respectively), it is not same for the transverse directions. (2,111) and (2,100) are exhibiting different slopes with the values of -534.32 and -269.82. This can be better spotted when a cross-section through 2-3 plane is analyzed. On that plane grain families have the same radii where their shapes resemble to the spherical inclusions as opposed to the tensile direction where the shapes resemble to needles as in Figure 4-6. Therefore, the interaction in between the grain orientations along transverse directions is too close to the results of the spherical inclusion with slopes of the (2,111) = -515.96, (2,100) = -270.59.

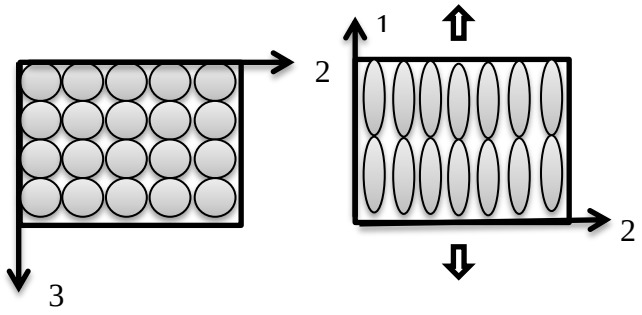

Figure 4.6. Cross sections of 2-3 and 1-2 planes of an aggregate constituted from fibers where 1 is the fiber axis.

On the other hand, along tensile direction the separation of the member stresses is more than the isostrain case. If we re-consider Equation 2.54 it can be seen that shrinkage or expansion of the curves is depending on the L^*(effective modulus) which depends on the eshelby tensor S and the overall modulus of the aggregate L. Since S is the output of the eshelby inclusion parameters, while having an inclusion of (1,1,1) leads to a shrinkage on the tensile direction, (15,1,1) leads to an expansion of the stresses on the grain-sets.

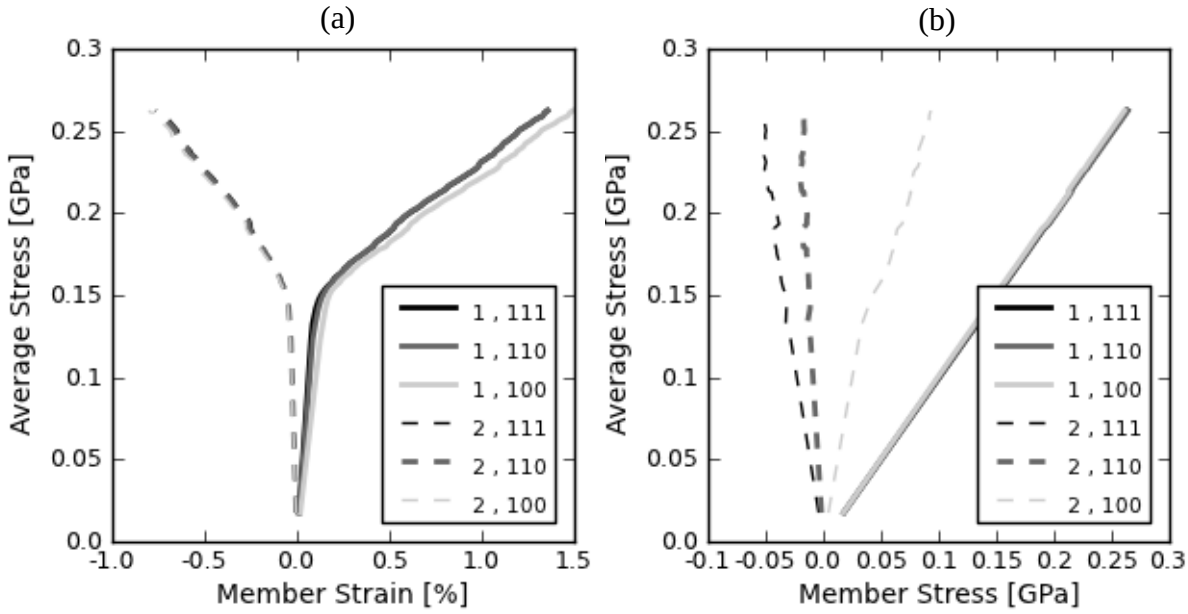

Figure 4.7. (a) Cluster average stress versus member strain on the specified (S,hkl) grain sets, (b) average stress versus member stress on the specified (S,hkl)grain sets. Eshelby interaction with an inclusion shape of (1,15,15) for single-phase Cu under uniaxial tension.

Case-5 is the model of the ellipsoidal inclusions with shapes (1,15,15). Representation of the layers of a single phase material is conducted with the disc-shaped inclusions. The axis ratios are selected such that discs are inserted in a plane perpendicular to the applied load as in Figure 4.8b in which the cross sections are featured. Having a radius of 15 along the axis-2 w.r.t. axis-1 brings the morphological effects. These effects can be seen in Figure 4.7. In Figure 4.7b stresses on the grain families (1,hkl) are on top of each other, representing an isostress behavior. This can be well explained by introducing the similarity in between the serially connected springs (see Figure 2.5b). Although elongations of the springs can differ according to their stiffnesses, they are all subjected to the same stress. Since the thickness of the inclusion along axis-1 is much less than other directions, planes of the inclusion can be thought as serially-placed inclusions along the loading direction (axis-1). As a result, strains along tensile axis diverge for the grain-sets more than the other eshelby inclusion shapes.

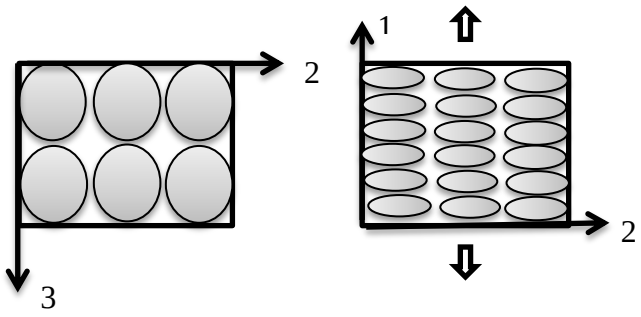

Figure 4.8. Cross sections of 2-3 and 1-2 planes of an aggregate constituted from disc-shaped grains.

As the last case of the single-phase materials, a strong <111> fiber texture of Cu is investigated. This case is prepared to create a basis for the further arguments that is hold in the multi-phase material section. In this texture, {111} crystallographic planes are aligned along the axis-1 in the sample coordinate system. Transverse directions are exhibiting a random distribution around the <111> direction; hence a transversely isotropic aggregate is organized. Inclusions are spherical. Since the texture is a strong <111> texture with a 0.92 volume fraction, it is expected to see overall behavior is directed by the (1,111) grains. Considering Figure 4.9b (1,111) curve exhibits a slope of 1.

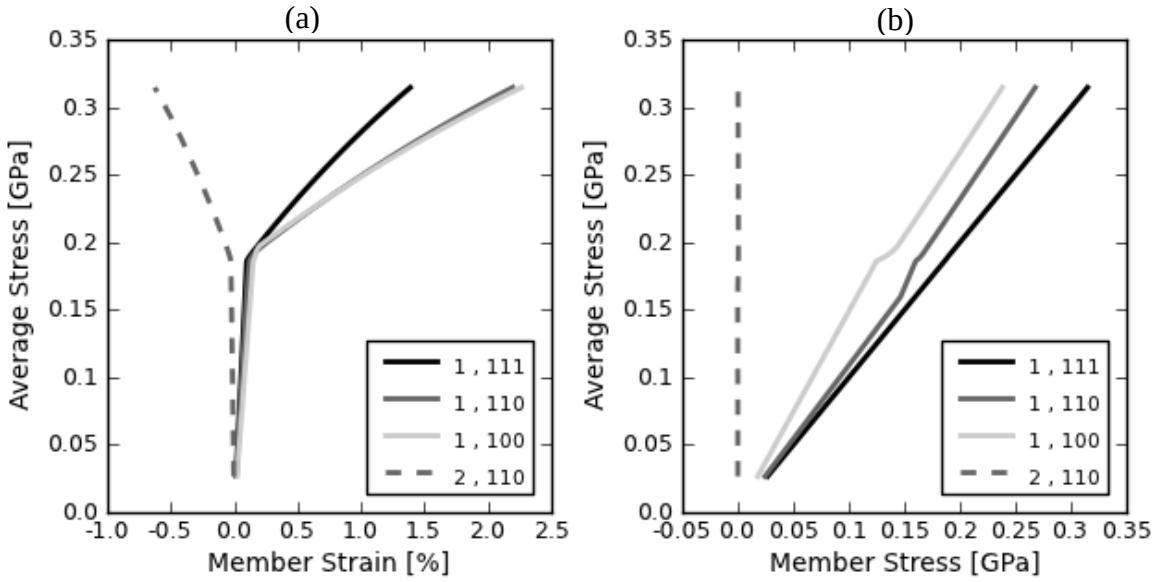

Figure 4.9. (a) Cluster average stress versus member strain, (b) average stress versus member stress on the specified (S,hkl) grain sets. Eshelby interaction with an inclusion shape of (15,1,1) for single-phase transversely isotropic Cu under uniaxial tension.

4.3. Multi-phase Self-consistent Models

APMF is also capable of modeling multi-phase materials. To exemplify, 4 cases are evaluated (case 7-10 in Table 4.1). Aggregates of Copper and Niobium are considered with different combinations of ellipsoidal shapes and orientations of phases in order to show the capabilities of the APMF. The results will be presented in two stages: First, to present the relative deformation/load that each phase bears on average, (entire) cluster stress versus average phase strain and cluster stress versus average phase stress plots are shown. Second, individual orientation sets are examined with member stress and strain plots in likeness to the previous sections. Average phase strain (ε_x) or stress (σ_x), where *x* = Cu, Nb, is calculated as the volume-fraction weighted average of all grains of phase *x*. Table 4.6 summarizes the load/strain sharing pattern of phases via phase apparent moduli and phase load fractions:

$$\bar{E}_x = \frac{d\sigma_{avg}}{d\varepsilon_{1,x}}, \qquad x = Cu, Nb \tag{4.5}$$

$$L_{f_x} = \frac{d\sigma_{1,x}}{d\sigma_{avg}}, \qquad x = Cu, Nb \tag{4.6}$$

Note that $v_{f_{Cu}} L_{f_{Cu}} + v_{f_{Nb}} L_{f_{Nb}}$ has to be equal to 1, where v_{f_x} is the volume fraction of Cu or Nb phase.

Table 4.6. Average phase properties of Cu and Nb, Apparent modulus, $\bar{E}_x$, Load fraction, $L_{f_{Cu}}$.

	$\bar{E}_{Cu}$	$\bar{E}_{Nb}$	$L_{f_{Cu}}$	$L_{f_{Nb}}$
Case7	121.70	112.01	1.03	0.97
Case8	118.91	110.74	1.05	0.86
Case9	117.69	100.96	1.06	0.95
Case10	NA	NA	1.19	0.81

4.3.1. Two-phase Random Mixture

This is the case sketched in Figure 1.4d corresponds to the case 7 in Table 4.1. Aggregates have random texture for both Copper and Niobium. Number of grains and volume fractions of phases are equal, 5000 and 0.5, respectively. Equiaxed grain geometry is considered with (1,1,1) Eshelby radii for all grains. Hardening parameters used in the model are tabulated in Table 4.3. Only one deformation system is considered for each phase: ($\{1\,1\,1\} < 1\bar{1}0 >$ slip for Cu, $\{1\,1\,0\} < \bar{1}\,1\,1 >$ slip for Nb.) The phase-average stress/strain plots in Figure 4.10 consider loading direction (axis 1) components only. Cluster average stress versus phase-averaged strains are plotted in Figure 4.10a. Cu and Nb phase-averaged strains have nearly the same elastic slope. On the other hand, load fractions are 1.03, 0.97 in Figure 4.10b, respectively. On average, Cu phase takes more stress than Nb due to the overall stiffness of the aggregate. For random texture equiaxed single phase Cu and Nb, Young's modulus is 129.7 and 105 GPa, respectively (Table 4.3).

The apparent values in Table 4.6 are pulled together with respect to these: 121.7 for Cu and 112 for Nb indicating the compromise imposed by the mixed self-consistent model.

Slip plasticity is initiated in the Copper phase first. This is apparent in Figure 4.10b, as the point Cu curve shoots up and crosses over the Nb curve. This is related to two factors: (i) Cu taking slightly more load in the elastic region due to its slightly higher stiffness, (ii) more importantly Cu slip having a smaller critical resolved shear stress with respect to that of Nb (Table 4.3)After Cu goes plastic, excess load is transferred to Nb, causing it to yield shortly afterwards. Since Cu is assumed to harden more than Nb (Table 4.3) Cu and Nb load-sharing (slopes in Figure 4.10b) tends to equilibrate in later stages of plasticity.

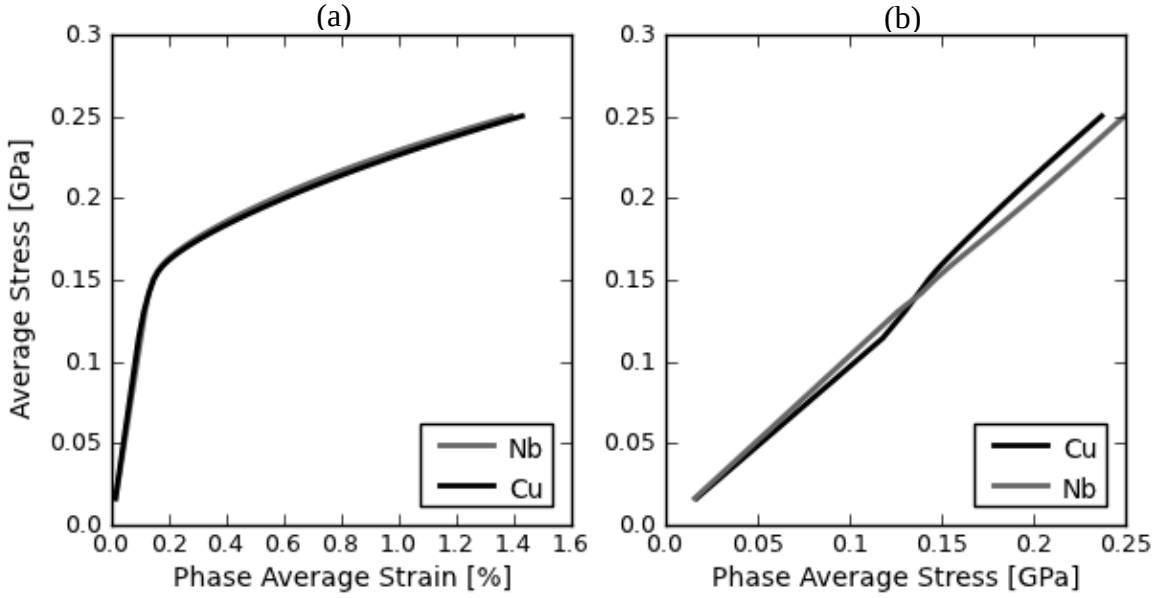

Figure 4.10. Phase average stress/strain curves of Cu and Nb equiaxed grain aggregates under uniaxial tension. (a) Cu+Nb cluster average stress versus individual phase strains, (b) Cu+Nb cluster average stress versus individual phase stresses.

For load sharing inside individual phases, it is worthwhile to investigate the grain subsets. In Figure 4.11, stress and strain of grain orientation families are plotted. As expected, inside an individual phase equivalent results are obtained with respect to the single phase run in Case 3 in Section 4.2. The only physical difference here is HEM being

composed by both Cu and Nb. However, since orientation distribution is random, HEM stiffness will come out as an isotropic tensor regardless. This Cu+Nb stiffness is further quite close to single phase Cu stiffness since Cu and Nb uniaxial moduli is within 6% of each other as shown before. Load fraction for the (1,111) is 1.19, (1,110) is 1.09 and (1,100) is 0.79. Difference in between the given fraction values and the values of Case 3 are 0.03. This constant difference is stemming from the contribution of the Niobium aggregate.

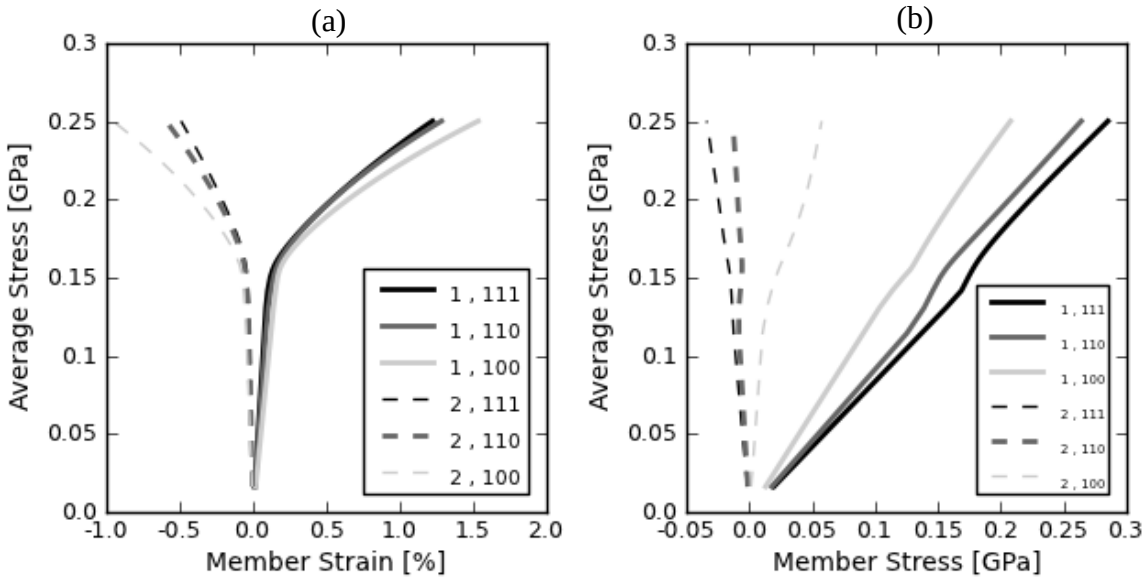

Figure 4.11. (a) Cluster average stress versus member strain, (b) average stress versus member stress on the specified (S,hkl) grain sets in the Cu phase of Cu+Nb cluster under uniaxial tension. Details in Table 4.1 case number 7.

Behavior inside the Nb aggregate is shown in Figure 4.12. Since BCC Nb has anisotropy ratio that is less than 1, its softest direction is <100> and stiffest is <111>, as opposed to Cu. As a result, slope of the stress-strain curve (1,111) is lower than the (1,100) curve in Figure 4.12a. Figure 4.12b, (1,100) grain sets carries 1.11 of the load where (1,111) carries 0.86. Slip plasticity is activated in (1,100) grains before the others. As stated in the Section 4.2, load is transferred to the less stiff grain sets. (1,111) grain sets are entering to the plastic zone when the curve (1,111) shifts upward.

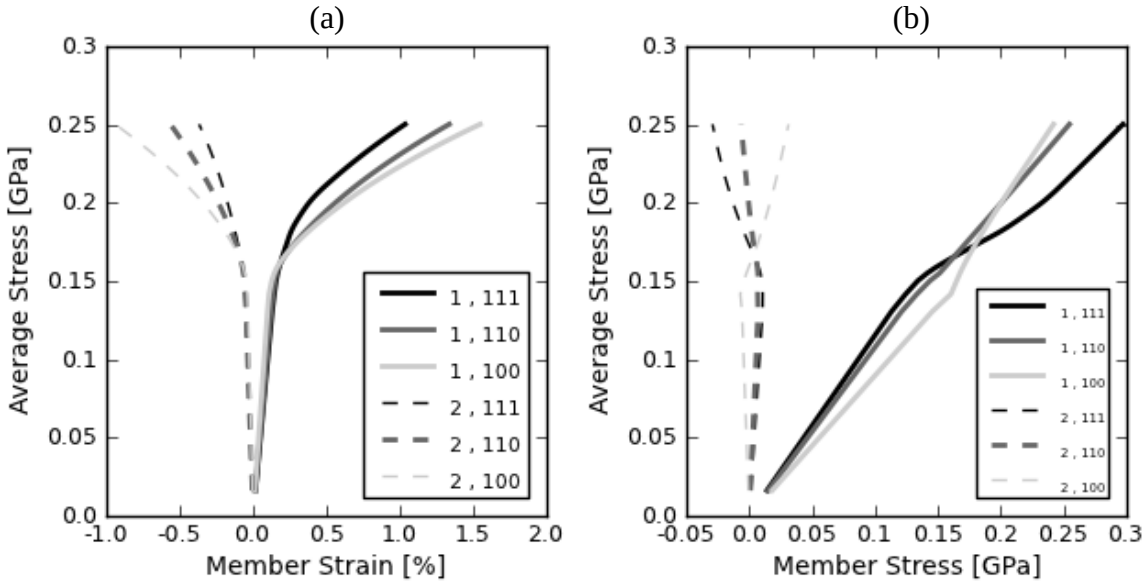

Figure 4.12. (a) Cluster average stress versus member strain, (b) average stress versus member stress on the specified (S,hkl) grain sets in the Nb phase of Cu+Nb cluster under uniaxial tension. Details in Table 4.1, case number 7.

4.3.2. Fiber Second-phase Inside Equiaxed First-phase

In the two-phase, fiber-matrix application, the morphologies in Figure 1.4e, h are aimed. Figure 1.4e corresponds to the case 8 in Table 4.1 with 5000 spherical (1,1,1) grains of Copper and 2500 needle-shaped grains (15,1,1) of Niobium. Volume fractions of phases are 0.75 for Cu and 0.25 for Nb. Niobium grain cluster has a wire drawing texture; the preferred orientation is such that <110> direction is aligned with the fiber axis [38]. Copper grains have random orientation, imitating a cast Cu matrix.

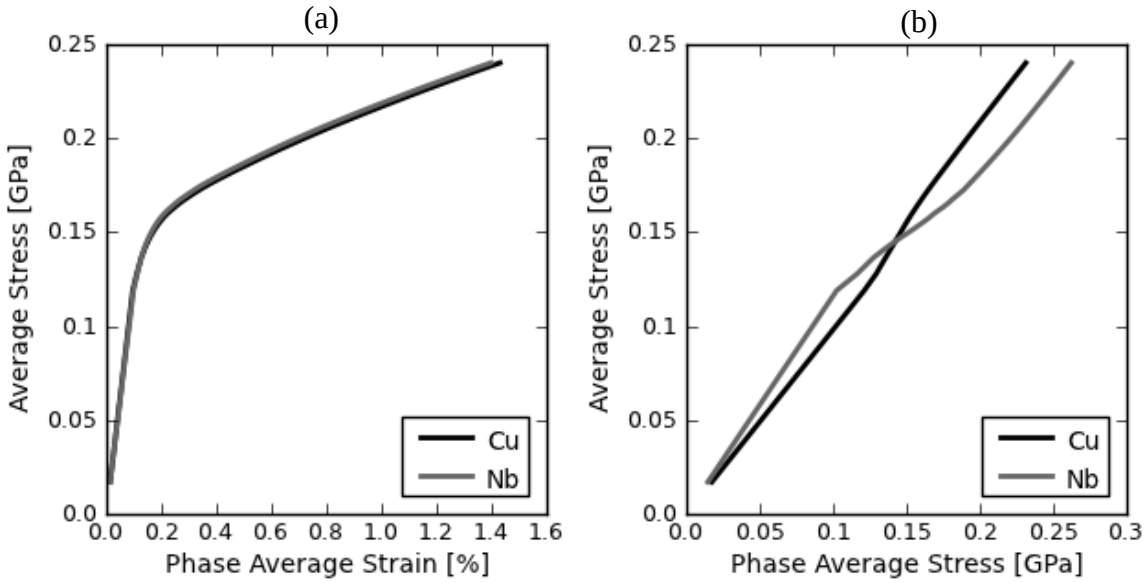

Figure 4.13. Phase average stress/strain curves of Cu equiaxed and Nb fiber grain aggregates under uniaxial tension. (a) Cu+Nb cluster average stress versus individual phase strains, (b) Cu+Nb cluster average stress versus individual phase stresses. Details in Table 4.1, case number 8.

The ninth case in Table 4.1 is a mixture of 5000 spherical (1,1,1) grains of Copper aggregate and 2500 fiber grains (15,1,1) of Niobium aggregate where the ellipsoids are rotated 45^o clockwise with respect to axis-1 and another 2500 fiber grains (15,1,1) of Niobium where the ellipsoids are rotated 45^o counterclockwise. Purpose is to mimic the behavior of a two phase material such that the fibers are placed with $\pm 45°$ orientation (somewhat in likeness to Figure 1.4h). One should note that this capability of introducing different ellipsoid axes is developed with APMF. So, this test case presents that capability as well. In Figure 4.15, $+45°$ Niobium aggregate is denoted as Nb1 and $-45°$ aggregate is denoted Nb2. Each Nb fiber has the <110> fiber texture described earlier. Volume fractions of Cu, Nb1 and Nb2 are 0.5, 0.25 and 0.25, respectively.

Recall, load/strain sharing parameters are summarized in Table 4.6 for the two-phase tensile tests. For case 9 Nb stands for the average of the two Nb fiber aggregates. In case 8 and 9, apparent modulus of the phases are expected to be equal. A representative 2D figure of the case is shown in Figure 4.14a where the Cu spherical grains are adjacent to the Nb

fiber grains. Load is along the long axis of the fiber shaped ellipsoid and ellipsoids have the small axis along the transverse direction (axis-2). Therefore, as explained in Section 4.2, interaction should be isostrain and apparent moduli are needed to be equal.

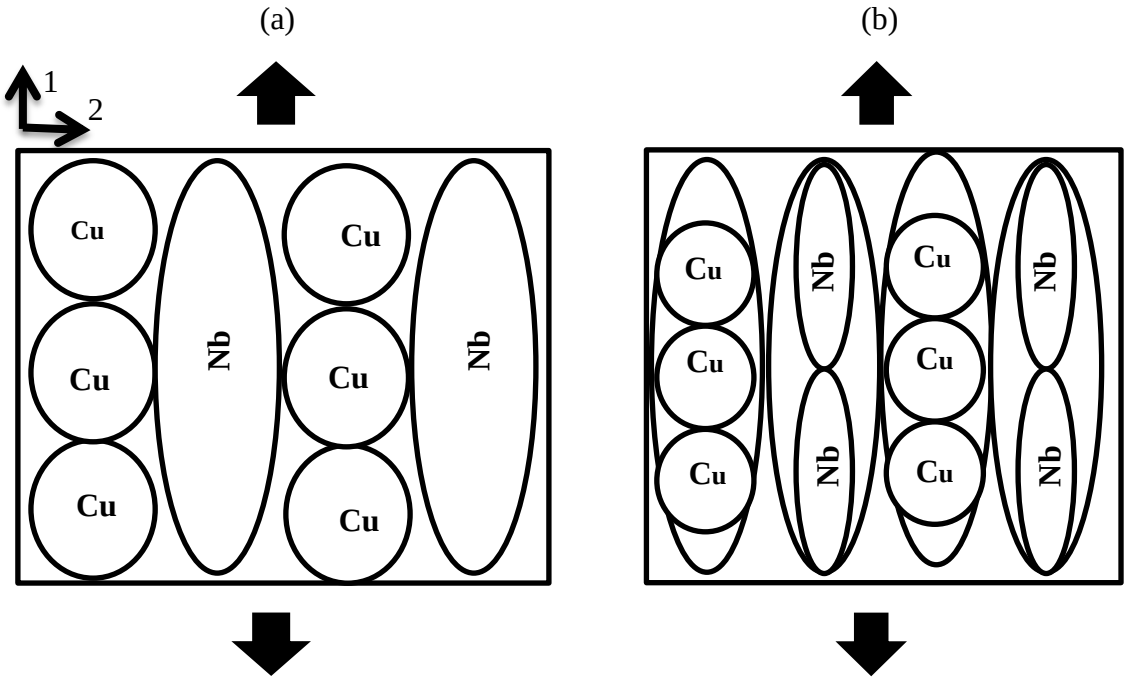

Figure 4.14. A schematic to depict a hierarchic model. (a) grains inside the cluster are interact directly without hierarchy, (b) First, load is shared among the fiber clusters of Cu and Nb grains. Second, each cluster dissipates the load onto its constituents.

This shows that the relation of the easy implementation of grain morphology and the Eshelby inclusion shapes for single phases is not applicable when the multi-phase material has different grain shapes. Case 8 and 9 are reflecting this phenomenon. Consequently, different grain shapes inside a common HEM leads incorrect interactions. This can be overcome by using hierarchical models as in Figure 4.14 b). Interaction first handled in between the Cu and Nb grain aggregates after this strain/stress is resolved individual Cu grains. This hierarchic calculation procedure is the future work of this study.

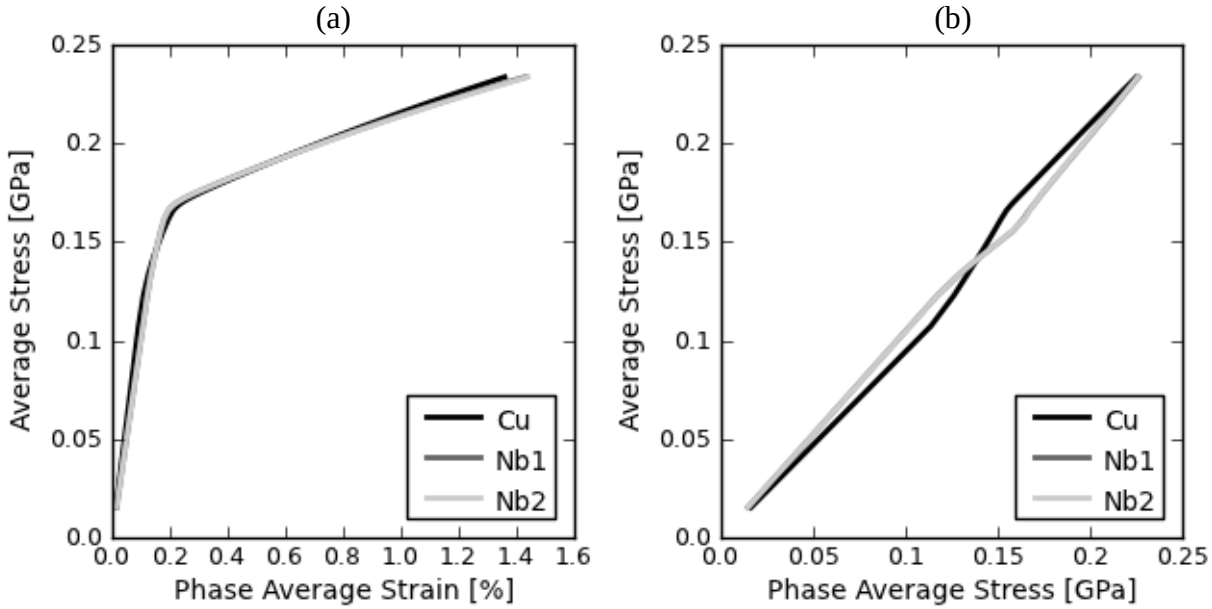

Figure 4.15. Phase average stress/strain curves of a Cu equiaxed grain and two families of Nb fiber grain aggregates under uniaxial tension. (a) Cu+Nb cluster average stress versus individual phase strains, (b) Cu+Nb cluster average stress versus individual phase stresses. Details in Table 4.1, case number 9.

4.3.3. Two-phase Multilayer

In this case, residual stresses inside a multi-layer material made up of alternating Cu and Nb layers, are modeled with APMF. This is modeled as a bilayer problem and the specifics are given Table 4.1 for case number 10. The layered morphology of Cu and Nb phases corresponds to Figure 1.4f. Each phase is modeled with 5000 grains with equal volume fractions. Since this case is inspired by physical-vapor-deposited Cu/Nb films; the texture of each phase is chosen in accordance: Cu and Nb have <111> and <110> film texture, meaning, <111>/<110> are aligned with the film normal for Cu/Nb. The fiber texture adopted in Figure 4.1 corresponds to this physical case. To impose strong in-plane compatibility (see Section 4.2), both phases are specified disc-shaped inclusions with Eshelby ellipsoid radii (15, 15, 1) where the film normal is axis-3. To impose the residual stress, thermal strain is imposed in Nb grains while the Cu-Nb cluster boundary conditions are stress-free. In this way, Cu and Nb grains will have to find middle ground due to the

imposed eigenstrain in the latter, always satisfying the condition that averaged residual stresses have to be zero.

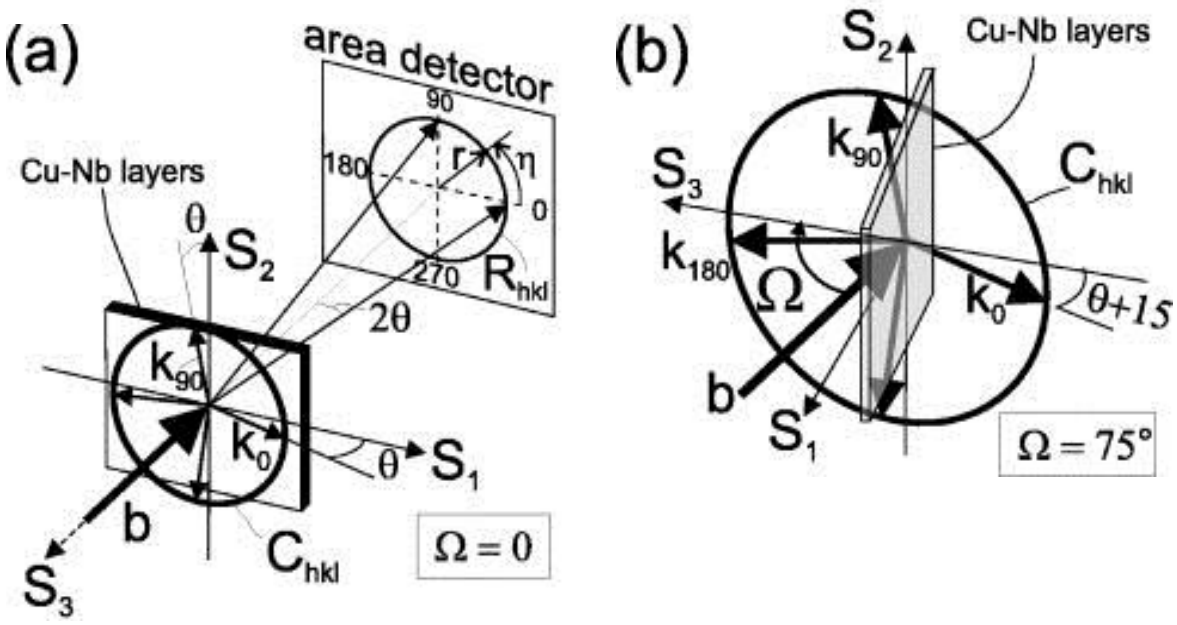

Figure 4.16. (a) Transmission geometry strain measurement with x-rays. (b) The configuration where the sample is rotated by Ω about S2 axis (reproduced from [11] with permission).

In order to investigate the residual strains inside the Cu-Nb sample, the data of a representative synchrotron x-ray experiment is simulated. The data collection directions **k** are shown in Figure 4.16 (the figure is from [11] ; which contains actual experimental data). X-ray beam is labeled as **b**. A columnar Cu-Nb layer thin film is firstly (i) placed perpendicular to the incident beam; secondly (ii) it is rotated to an angle Ω around S_2 where the S_1, S_2, S_3 are the sample coordinate axes. Each time, intensity information of the orientations is extracted from the area detector. On the area detector each ring corresponds to a Bragg reflection *hkl*. η is defined as the azimuthal angle in each ring. The strain data at each η is the average normal strain of the (hkl, k_η) orientation set along direction k_η. For example, strains normal to vector $\mathbf{k}_0$ are measured from the $\eta = 0$ neighborhood of an *hkl* ring.

Cu {110}, Cu {111} and Nb {110}, Nb {211} elastic strains are plotted against azimuthal angles for sample rotations Ω= 0^o, 60^o, (70^o, 75^o) and bottom plots are for the corresponding normalized intensities of the contributing grain sets in Figure 4.17-Figure 4.20. Intensity plot of the grain sets contributing to the strain at Ω=0 are not shown in the plots. Each point on the above plots is the elastic strains along k_η **(**Figure 4.16**)** versus azimuthal angles η. Although, the maximum deviation from ideal film texture is limited to about $\psi = 10°$ degrees as shown in Figure 4.1; and orientations with higher deviations are precluded physically; the entire orientation space is covered in the texture specifications to present continuous strain curves.

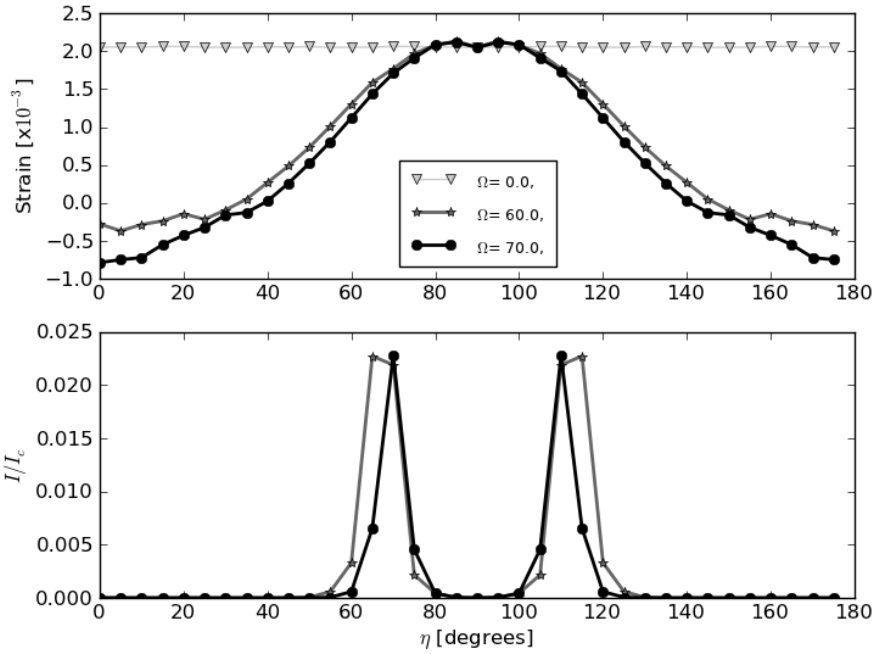

Figure 4.17. Cu {111} strains inside the Cu+Nb cluster plotted against each azimuthal angle for sample rotations Ω=0,60,70. The bottom plot shows the volume fractions of grain orientations that correspond to each azimuthal angle and uniform Ω=0 I/I_c is not shown.

In Figure 4.17 and Figure 4.18 at Ω= 0^o Cu {111} and {110} grains are randomly distributed. Therefore, strains on the grains for each azimuthal angle are same (not the primary reason). In the physical picture of residuals stress, Cu grains exhibit tension in the

plane($\varepsilon_{11} = \varepsilon_{22} = \varepsilon_m; \varepsilon_{12} = 0$). Since the Nb is thermally expands, Cu grains hinder the expansion of the Nb. Struggle in between Cu-Nb results in that Cu grains feel tension in reverse to the Nb grains, see Figure 4.19.

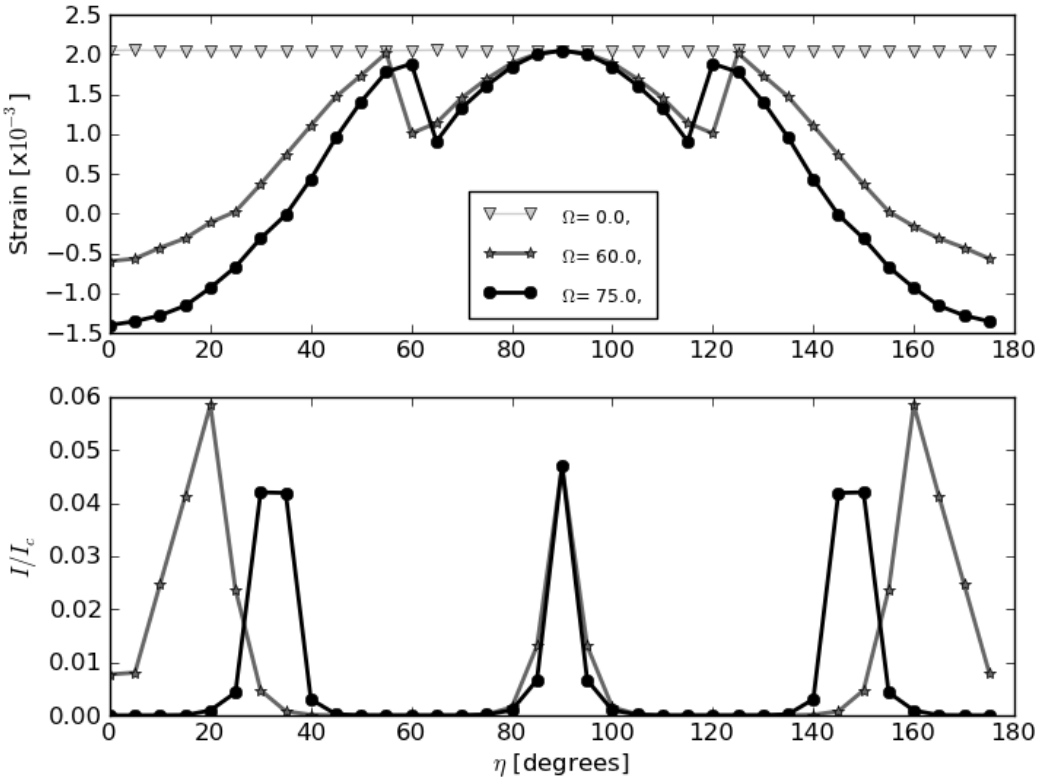

Figure 4.18. Cu {110} strains inside the Cu+Nb cluster plotted against each azimuthal angle for sample rotations Ω=0,60,70. The bottom plot shows the volume fractions of grain orientations that correspond to each azimuthal angle and uniform Ω=0 I/I_c is not shown.

The strains determined along the diffraction vectors $\mathbf{k}_0$, $\mathbf{k}_{180}$ are close to the strain in the film normal direction for Ω=75, see Figure 4.16.b. Conversely, $\mathbf{k}_{90}$, that is nearly coincident with the sample rotation axis S_2 remains in the plane of the film regardless of the sample rotation Ω. In Figure 4.19 and Figure 4.20 it is seen that the in-plane elastic strains are the same and Nb grains experiences compression, due to the poisson effect. Therefore for Ω=60,75 while $\mathbf{k}_0$ and $\mathbf{k}_{180}$ have positive normal strains $\mathbf{k}_{90}$ exhibits negative

normal strain. Since the rotation axis is S_2 and it is not changing during rotation in-plane strains at $\eta = 90°$ are coincident in all plots.

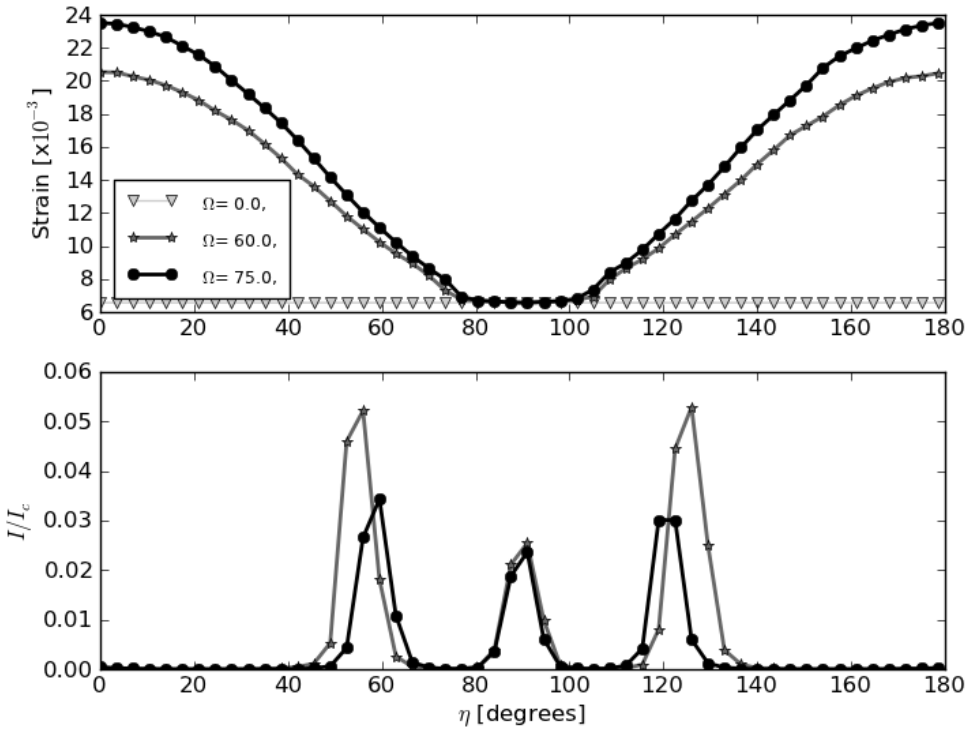

Figure 4.19. Nb {110} strains inside the Cu+Nb cluster plotted against each azimuthal angle for sample rotations Ω=0,60,75. The bottom plot shows the volume fractions of grain orientations that correspond to each azimuthal angle and uniform Ω=0 I/I_c is not shown.

The paper in [11] considers a Vook-Witt [39] model that does not have any complex interaction. Vook-Witt model is a selective combination of isostress and isostrain interactions. It basically imposes isostrain in the plane of the film and isostress in the remaining. If all the grains have the same strain tensor as in isostrain assumption, normal strains of any *hkl* plane inside a grain exhibits a sinusoidal relation with the applied strain. Different from isostrain model, Vook-Witt model gives freedom to the out of plane strains. In case 10 using a (15,15,1) Eshelby inclusion shape enables to have a close response to the Vook-Witt model. When (1-2) cross-section is compared with the third direction of the

cluster, isostress behavior along the third direction and isostrain response in the plane is observed as mentioned in Section 4.1.

$$\varepsilon_{11} = \varepsilon_{22} = \varepsilon_m, \varepsilon_{12} = 0; \sigma_{33}, \sigma_{23}, \sigma_{13} = 0 \tag{4.7}$$

As a result curves inside the strain versus azimuthal angle plots deviates from perfect sinusoidal curves as in Figure 4.17- Figure 4.22. This model was developed to describe strains in transversely isotropic thin films [39,40]. In the tenth case if Eshelby ellipsoids of (1,1,1) is used for both Cu and Nb then the hump around 90^o could not be seen. This is due to the struggling is carried to the in-plane to out of plane.

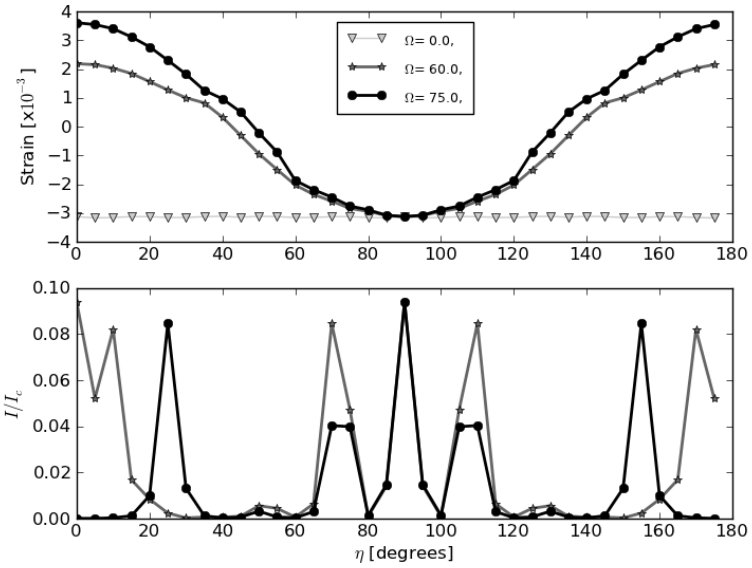

Figure 4.20. Nb {211} strains inside the Cu+Nb cluster plotted against each azimuthal angle for sample rotations Ω=0,60,75. The bottom plot shows the volume fractions of grain orientations that correspond to each azimuthal angle and uniform Ω=0 I/I_c is not shown.

Single phase runs with the equibiaxial in-plane strain boundary conditions given to the Cu and Nb individually (same texture and morphology for the case 10). {111} strain versus azimuthal angle plots are in Figure 4.21 and the same is conducted for the Nb for {110} in Figure 4.22. In conclusion, these single-phase runs confirm the case 10 by reflecting the same shapes an in the above figures for obtained.

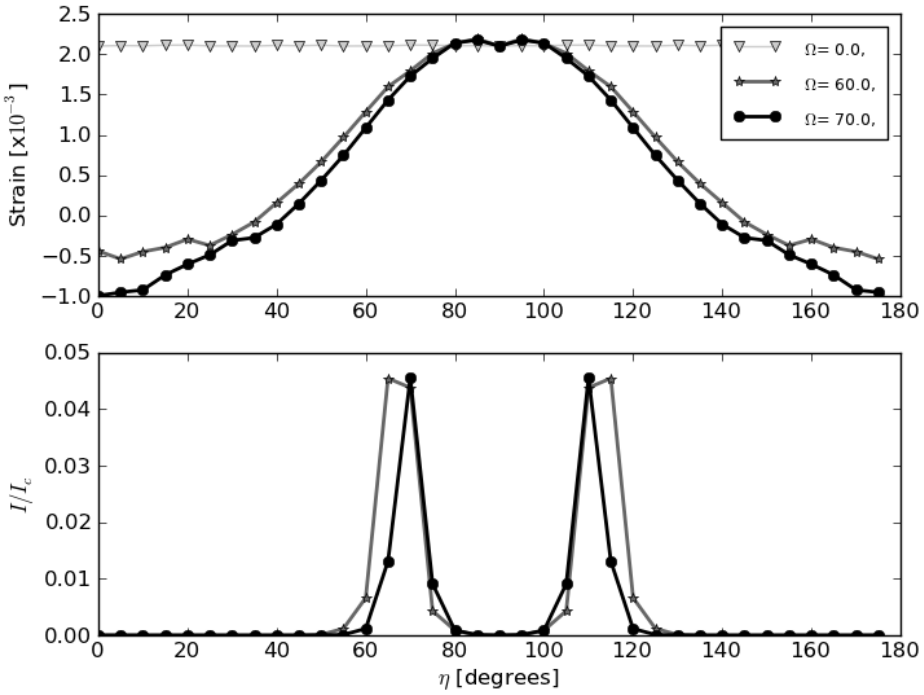

Figure 4.21. Single phase Cu {111} strains plotted against each azimuthal angle for sample rotations Ω=0,60,70. The bottom plot shows the volume fractions of grain orientations that correspond to each azimuthal angle and uniform Ω=0 I/I_c is not shown.

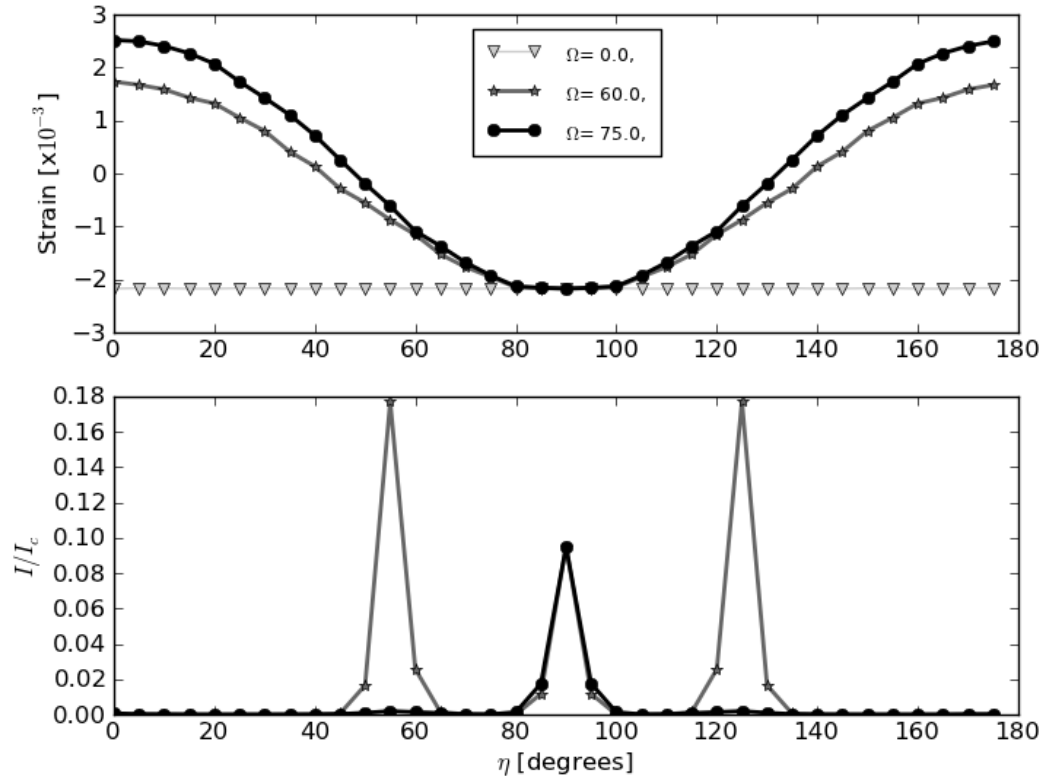

Figure 4.22. Single-phase Nb {110} plotted against each azimuthal angle for sample rotations Ω=0,60,75. The bottom plot shows the volume fractions of grain orientations that correspond to each azimuthal angle and uniform Ω=0 I/I_c is not shown.

5. CONCLUSION

Morphological evaluations of the 1-site polycrystalline deformation models are conducted for both single and multi-phase materials. Response of the material is governed by two main relations: constitutive law and interaction rule. By selective combination of both laws, a wide range of polycrystal problems can be successfully modeled. Here, an object-oriented software package has been developed where interchanging these model components is simple. This new framework has been called APMF (Adaptable Point Model Framework) and utilizes a combination of Python and FORTRAN languages.

To exceed the restrictions of straightforward 1-site models, APMF is developed such that interaction rules that are not yet implemented (such as 2-site model) or new constitutive rules (e.g., complex hardening types of slip plasticity) are introduced easily. In a way, APMF is a package that forms a working model with standardized preprocessing, postprocessing and data base interaction. The self-consistent model implementation of APMF is capable of evaluating multi-phase materials and ability to impose differing Eshelby ellipsoid radii/orientation for each grain. In the duration of this study, APMF has been tested by three interaction models isostrain, isostress, and self-consistent model.

Among these, only self-consistent model has a limited capability of mimicking morphological microstructures through the use of Eshelby ellipsoidal inclusion radii/orientations. This has been the main tool in evaluating various morphological test cases. By using limiting shapes of Eshelby ellipsoid (namely, sphere, needle, and disc) and comparing with the simplistic isostress/strain rules, the aim is to simulate the effect of structured (non-random) morphologies on the behavior of the polycrystals. Results are interpreted at the meso-scale with the stress/strain comparison of different grain orientation families.

First, the effect of needle and disc-shaped grains are characterized in a single-phase material. Provided both are aligned with the load axis, needle inclusion approximates an isostrain interaction whereas disc-shaped inclusion approximates an isostress interaction.

However, different from these simplistic models, these hold only in the loading direction and the grains compete in a complex manner in the transverse directions. It is concluded that there is a one-to-one correspondence between ellipsoid shape and nominal grain shape in a single-phase material. However, a multi-phase example of Nb fibers inside Cu spherical grain matrix does not exhibit one-to-one correspondence.

Second, simulation of two-phase structures is considered. The test cases are derived from two heavily-textured real-life structures: fiber-reinforced materials and multi-layers. It is concluded that the relation of the one-to-one implementation of grain morphology and Eshelby inclusion shapes for single phases is not applicable when the multi-phase material has different grain shapes. This can be overcome by including a hierarchic modeling. Firstly an isostrain interaction should be applied to the Cu grain families and Nb grain families. Secondly, Eshelby interaction should be hold inside the Cu aggregate having the isostrain boundary conditions on top. For the multilayer case, residual strains inside a Cu-Nb thin film are investigated introduced in the model by thermal straining of one of the phase. Strong in-plane compatibility is imposed with disc-shaped ellipsoids. Results are consistent with single-phase Cu and Nb simulations. It is observed that Vook-Witt assumption is valid for the bi-layer problems.

REFERENCES

1. Stevens, S. S., "On the Theory of Scales of Measurement", *Science,* Vol. 103, No. 2684, pp. 677-680, 1946.

2. Lubliner, J., "A Simple-Model of Generalized Plasticity", *International Journal of Solids and Structures,* Vol. 28, No. 6, pp. 769-778, 1991.

3. Lienert, U., T. S. Han, J. Almer, P. R. Dawson, T. Leffers, L. Margulies, S. F. Nielsen, H. F. Poulsen and S. Schmidt, "Investigating the Effect of Grain Interaction During Plastic Deformation of Copper", *Acta Materialia,* Vol. 52, No. 15, pp. 4461-4467, 2004.

4. Bishop, J. F. W. and R. Hill, "A Theoretical Derivation of the Plastic Properties of a Polycrystalline Face-Centred Metal", *Philosophical Magazine,* Vol. 42, No. 334, pp. 1298-1307, 1951.

5. Castelnau, O., P. Duval, R. A. Lebensohn and G. R. Canova, "Viscoplastic Modeling of Texture Development in Polycrystalline Ice with a Self-Consistent Approach: Comparison with Bound Estimates", *Journal of Geophysical Research-Solid Earth,* Vol. 101, No. B6, pp. 13851-13868, 1996.

6. Hutchinson, J. W., "Elastic-Plastic Behaviour of Polycrystalline Metals and Composites", *Proceedings of the Royal Society of London, Series A (Mathematical and Physical Sciences),* Vol. 319, No. 1537, pp. 247-272, 1970.

7. Lebensohn, R. A., P. A. Turner and G. R. Canova, "Recent Advances in Modelling Polycrystals with Complex Microstructures", *Computational Materials Science*, Vol. 9, No. 1–2, pp. 229-236, 1997.

8. Roters, F., P. Eisenlohr, T. R. Bieler and D. Raabe, *Crystal Plasticity Finite Element Methods,* Wiley-VCH Verlag GmbH & Co. KGaA, 2010.

9. Eshelby, J. D., "The Determination of the Elastic Field of an Ellipsoidal Inclusion, and Related Problems", *Proceedings of the Royal Society of London Series a-Mathematical and Physical Sciences*, Vol. 241, No. 1226, pp. 376-396, 1957.

10. Misra, A. and H. Kung, "Deformation Behavior of Nanostructured Metallic Multilayers", *Advanced Engineering Materials*, Vol. 3, No. 4, pp. 217-222, 2001.

11. Aydiner, C. C., D. W. Brown, A. Misra, N. A. Mara, Y. C. Wang, J. J. Wall and J. Almer, "Residual Strain and Texture in Free-Standing Nanoscale Cu-Nb Multilayers", *Journal of Applied Physics*, Vol. 102, No. 8, 2007.

12. Misra, A., J. P. Hirth and R. G. Hoagland, "Length-Scale-Dependent Deformation Mechanisms in Incoherent Metallic Multilayered Composites", *Acta Materialia*, Vol. 53, No. 18, pp. 4817-4824, 2005.

13. Bishop, J. F. W. and R. Hill, "A Theory of Plastic Distortion of a Polycrystalline Aggregate under Combined Stresses", *Philosophical Magazine*, Vol. 42, No. 327, pp. 414-427, 1951.

14. Kroner, E., "On the Plastic Deformation of Polycrystals", *Acta Metallurgica*, Vol. 9, No. 2, pp. 155-161, 1961.

15. Budianski, B. and T. T. Wu, "Theoretical Prediction of Plastic Strains of Polycrystals", *Proc. of the 4th U.S. National Congress of Applied Mechanics*, Vol., No. pp. 1175, 1962.

16. Hill, R., "The Essential Structure of Constitutive Laws for Metal Composites and Polycrystals", *Journal of the Mechanics and Physics of Solids*, Vol. 15, No. 2, pp. 79-95, 1967.

17. Lin, T. H., "Analogy between Body Force and Inelastic Strain Gradient in Cubic Crystals and Isotropic Bodies", *Proceedings of the National Academy of Sciences of the United States of America*, Vol. 55, No. 3, pp. 477-&, 1966.

18. Kocks, U. F., Tome, C.N., Wenk, H-R. , *Texture and Anisotropy*, Cambridge University, New York, 1998.

19. Nemat-Nasser, S., "Multi-Inclusion Method for Finite Deformations: Exact Results and Applications", *Materials Science and Engineering: A,* Vol. 285, No. 1–2, pp. 239-245, 2000.

20. Clausen, B., T. Lorentzen and T. Leffers, "Self-Consistent Modelling of the Plastic Deformation of Fcc Polycrystals and Its Implications for Diffraction Measurements of Internal Stresses", *Acta Materialia,* Vol. 46, No. 9, pp. 3087-3098, 1998.

21. Kocks, U. F., C. N. Tomé and H.-R. Wenk, *Texture and Anisotropy : Preferred Orientations in Polycrystals and Their Effect on Materials Properties*, Cambridge University Press, Cambridge, U.K., New York, 1998.

22. Freund, L. B. and S. Suresh., *Thin Film Materials*, Cambridge University Press, 2004.

23. Shea, J. J., "Microstructural Characterization of Materials [Book Reveiw]", *Electrical Insulation Magazine, IEEE,* Vol. 16, No. 2, pp. 38, 2000.

24. Brandon, D. G. and W. D. Kaplan, *Microstructural Characterization of Materials*, J. Wiley, Chichester, 1999.

25. Cavaliere, P., "Mechanical and Microstructural Behaviour of 6061/Al", *Multidiscipline Modeling in Materials and Structures,* Vol. 2, No. 4, pp. 449-461, 2006.

26. Callister, W., Rethwisch D., *Materials Science and Engineering: An Introduction*, 8 ed., Wiley, 2010.

27. G.I., T., *The Journal of the Institute of Metals,* Vol. 62, pp. 307, 1938.

28. Havner, K. S., "Comparisons of Crystal Hardening Laws in Multiple Slip", *International Journal of Plasticity,* Vol. 1, No. 2, pp. 111-124, 1985.

29. Hill, R., "The Elastic Behaviour of a Crystalline Aggregate", *Proc. Phys. Soc. London* Vol. A 65, No. pp. 349-354, 1952.

30. Barton, G., *Elements of Green's Functions and Propagation: Potentials, Diffusion, and Waves*, Clarendon Press, New York, 2005.

31. Aki, K. and P. G. Richards, *Quantitative Seismology*, University Science Books, Sausalito, CA, 2009.

32. Phillips, R., *Crystals, Defects and Microstructures: Modeling across Scales*, Cambridge University Press, Cambridge, 2001.

33. Withers, P. J., W. M. Stobbs and O. B. Pedersen, "The Application of the Eshelby Method of Internal Stress Determination to Short Fibre Metal Matrix Composites", *Acta Metallurgica*, Vol. 37, No. 11, pp. 3061-3084, 1989.

34. Brown, D. W., M. A. M. Bourke, B. Clausen, T. M. Holden, C. N. Tome and R. Varma, "A Neutron Diffraction and Modeling Study of Uniaxial Deformation in Polycrystalline Beryllium", *Metallurgical and Materials Transactions A (Physical Metallurgy and Materials Science),* Vol. 34A, No. 7, pp. 1439-49, 2003.

35. Clausen, B., T. Lorentzen, M. A. M. Bourke and M. R. Daymond, "Lattice Strain Evolution During Uniaxial Tensile Loading of Stainless Steel", *Materials Science and Engineering A,* Vol. 259, No. 1, pp. 17-24, 1999.

36. Daymond, M. R., M. Preuss and B. Clausen, "Evidence of Variation in Slip Mode in a Polycrystalline Nickel-Base Superalloy with Change in Temperature from Neutron Diffraction Strain Measurements", *Acta Materialia,* Vol. 55, No. 9, pp. 3089-3102, 2007.

37. Alted F., V. I., "Hierarchical Datasets in Python," 2002-2009, http://www.pytables.org/, Accessed March 2013.

38. Heussner, R. W., P. J. Lee, P. D. Jablonski and D. C. Larbalestier, "The Influence of Niobium and Niobium-Titanium Grain-Size on the Drawing Instability of Niobium Diffusion-Barriers in Niobium-Titanium Wire", *Advances in Cryogenic Engineering, Vol 40, Pts a and B,* Vol. 40, No. pp. 755-762, 1994.

39. Vook, R. W. and F. Witt, "Thermally Induced Strains in Evaporated Films", *Journal of Applied Physics,* Vol. 36, No. 7, pp. 2169-&, 1965.

40. Leoni, M., U. Welzel, P. Lamparter, E. J. Mittemeijer and J. D. Kamminga, "Diffraction Analysis of Internal Strain-Stress Fields in Textured, Transversely Isotropic Thin Films: Theoretical Basis and Simulation", *Philosophical Magazine a-Physics of Condensed Matter Structure Defects and Mechanical Properties,* Vol. 81, No. 3, pp. 597-623, 2001.